Permian Granitic Plutons from the Northern Margin of the North China Craton: Implications for the Tectonic Evolution of the Central Asian Orogenic Belt

Jingsheng Chen , Dexin Tian , Bin Li * , Zhonghui Gao , Weiwei Li , Chao Zhang , Yan Wang

Posted Date: 21 September 2023

doi: 10.20944/preprints202309.1383.v1

Keywords: Permian granitoids; Zircon U-Pb Geochronology; Geochemistry; Tectonic evolution; Northern Margin of the North China Craton

Article

Permian Granitic Plutons from the Northern Margin of the North China Craton: Implications for the Tectonic Evolution of the Central Asian Orogenic Belt

Jingsheng Chen [1,2] , Dexin Tian [3], Bin Li [1,2]*, Zhonghui Gao [4], Yi Tian [4], Weiwei Li [4], Chao Zhang [1,2] and Yan Wang [1,2]

[1] Shenyang Geological Survey Center of China Geological Survey, Shenyang 110034, China
[2] Northeast Geological S&T Innovation Center of China Geological Survey，Shenyang 110034，China
[3] Non-Ferrous Metals Geological Exploration Bureau of Zhejiang Province, Shaoxing 312000, China
[4] Institute of Geology and Mineral Resources of Liaoning Co., Ltd. Shenyang, 110029, China

Abstract: As the largest accretionary orogen in the world, the Central Asian Orogenic Belt (CAOB) has continuous juvenile crustal growth in the Phanerozoic. The northern margin of the North China Craton(NCC) and its adjacent area is the eastern segment of the CAOB, and is a key area to study the geological evolution of Paleo-Asian Ocean (PAO). In the Permian, the west of the northern margin of NCC belongs to a post-collision extensional environment, and the east belongs to a subduction stage. But, As a connecting area, the Permian evolution of PAO in the middle of northern margin of NCC has not been systematically studied. In order to fill the blank and understand the temporal and spatial continuous evolution process of PAO, this paper focused on the Permian granitic rocks in the Chifeng area, zircon U-Pb dating and the geochemical analysis of the whole rock main and trace elements were conducted in order to build a granite chronological framework, discuss the genesis and tectonic background of the granite rocks as well as the magma-tectonic evolution history in the Chifeng area. Zircon U-Pb dating results of 8 samples are 269±1 Ma, 268±3 Ma, 260±4 Ma, 260±1 Ma, 260±1 Ma, 255±2 Ma, 254±2 Ma, 256±1Ma, which showed that the Permian granitic rocks had undergone three stages of emplacement: (1) The monzogranite and syenite (294-284 Ma); (2) The monzogranite (269-260Ma) and (3) The monzogranite and syenite (256-254Ma). The Middle Permian magmatism (269-260Ma) was represented by the monzogranite assemblages with different grain sizes. The geochemical characteristics showed that they were high-potassium calc-alkaline-potassium dossonite series of granites formed in compressional environment, indicating there was a collision between the Xing'an-Mongolian Orogenic Belt (XMOB) and the North China Craton (NCC). During the Late Permian-Early Triassic (256-248Ma), the granites in the Chifeng area are dominated by the A-type and I-type granites of high-potassium calc-alkaline series formed under an extensional environments, which constituted typical "bimodal" rock assemblage combined with the coeval basic rocks, suggesting the study area was in an extensional environment where the subducting slab is fragmented during the collision between the XMOB and the NCC. According to emplacement time and occurrence location, the plutons are interpreted to have been generated by the subduction-collision of the Paleo-Asian oceanic crust beneath the NCC. This study provides strong evidence for Permian tectonic evolution and the characterization of the eventual closure of the Paleo-Asian Ocean in the Chifeng City at the northern margin of the NCC.

Keywords: permian granitic pluton; geochronology; geochemistry; tectonic evolution of the paleo-asian ocean; northern margin of the North China Craton

Preprints (www.preprints.org) | NOT PEER-REVIEWED | Posted: 21 September 2023 doi:10.20944/preprints202309.1383.v1

1. Introduction

As the largest Phanerozoic subduction-accretion orogen, the Central Asian Orogenic Belt (CAOB) is located between the Siberian Plate (SP) and the North China Craton (NCC). Its formation is closely related to the evolution of the Paleo-Asian Ocean（PAO）（Sengör and Natal'in，1996；Sengör et al., 1993；Jahn，2004）. The CAOB adjacent to the northern margin of the NCC is also known as the Xing'an-Mongolian Orogenic Belt (XMOB), which is the orogenic belt with the longest evolutionary history and the most complicated tectonic and magmatic activities in China(Figure 1a). Its formation is related to the closure of the PAO. Continental crust accretion and extensive and long-lasting tectonic-magmatic activities took place throughout the Phanerozoic（Li et al.,2006；Wu et al.,2011）. As a result, microcontinents and Phanerozoic orogenic belts of different periods formed the XMOB(Wu et al.,2002). After intense continental transformation and multi-stage geological evolution, the XMOB had complex and diverse structure and crustal material composition, rich in oil and gas and metal mineral resources, which was a natural laboratory to study continental dynamic evolution, magmatism and metallogenic mechanism of metal elements for the scholars of China and abroad（Li et al., 2006）.

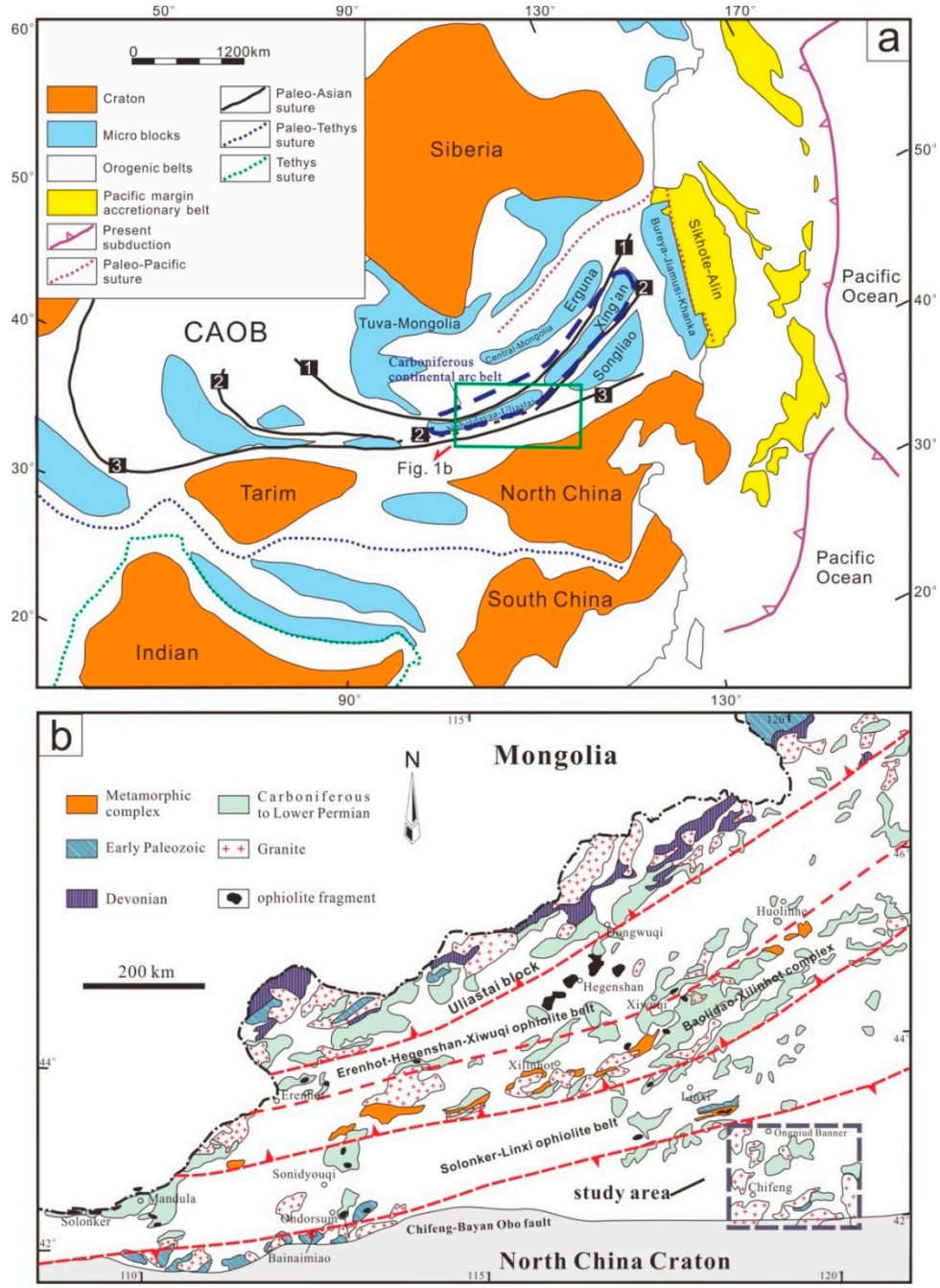

 doi:10.20944/preprints202309.1383.v1

Figure 1. (a) Schematic tectonic map showing main tectonic subdivisions of central and eastern Asia and location of northeast China (modified from Li, 2006); (b) Simplified geological map of the central Inner Mongolia of the CAOB showing tectonic units (modified from Song et al., 2015 ; Chen et al., 2019).

Geologists have conducted in-depth studies on the evolution of the PAO through different methods. They consider that the PAO has experienced a long evolutionary process. As the mid-ocean ridge gradually expands and the ocean opens to its maximum range, the oceanic crust begins to subduct towards the continents on both sides. The PAO basins shrank and gradually closed. The micro-continents between the two large plates began to collide and merge. Finally, the PAO disappeared and the two continental plates collided and sutured. After the collision, it entered the post-orogenic stage of stress relaxation, and a series of complex continental crust geological transformation events began to occur, including extension and extension, structural collapse, and stress delamination（Chen et al., 2009；Wang., 2014；Chen et al., 2022a）. More and more data proves that the Solonker-Xar Moron-Changchun-Yanji Suture (SXCYS) is the final location where the two major plates collide and join together（Xiao et al., 2003；Zhang，et al., 2009a；Song et al., 2015；Zhao et al., 2016；Liu et al., 2017；Liu et al., 2015）. Currently, the focus of debate is the time of collision and suture, including the following four main points of view:

(1) Based on the analysis of sedimentary petrography, the mixed accumulation of ophiolite, the formation of stratigraphic deposition, and the contact between the Carboniferous strata and the ophiolite, some scholars believe that the northern margin of the NCC and the XMOB collided and collaged in the early Late Paleozoic, resulting in the disappearance of the PAO. Since the Late Carboniferous, the study area has been characterized by intracontinental rifting magmatic and sedimentary activities after the SP and the NCC were united through the XMOB（Tang，1990；Tang et al., 2022）. It is believed that the Permian basin is a new rift basin with extensional volcanic activities（Tang，1990；Hendrix et al., 1996）. Some scholars also believe that the PAO closed before the Early Permian based on magmatism（Zhao et al., 2016；Zhang et al., 2014）.

(2) Based on the study on the Early-Middle Permian alkaline granites in the northern margin of the NCC, some scholars consider that the time limit for the final merging of the northern margin of the NCC and the XMOB is the Early-Middle Permian（Zhang et al., 2007；Wang., 2014；Zhang et al., 2009a；Li et al., 2018）.

(3) Some scholars consider that the subduction of the PAO occurred in the Late Paleozoic, and its final extinction occurred during Late Permian-Early Triassic. There were many evidences for this point of view: ①Based on paleomagnetism, mixed paleontological groups and biological extinction events, it was inferred that the PAO between the two plates finally closed at the end of the Permian（Sengör et al., 1993；Wang and Liu，1986； Li et al.,2009）; ②The evidence from magmatic rock chronology and geochemistry showed that it was post-collision extensional environment in the Early Triassic. Therefore, the closure of the PAO was deliminated as Late Permian（Li，2006；Xiao et al., 2003；Zhang et al., 2006；Windley et al. 2007；Guan et al., 2018; Shi et al., 2022; Chen et al. 2019, 2022b）; ③ Carboniferous oceanic crust basalts and Permian radiolarian siliceous were discovered in the north of Xar moron River（Wang., 2001；Li et al., 2007）. The reefs and marine fossils of the late Permian and the P/T unconformity surface exposed in Balin Right Banner in Inner Mongolia and Jiutai County in Jilin proved that PAO closed at the end of the Late Permian（Tian et al., 2016）; ④ Ophiolite suites formed in the Late Permian-Early Triassic in the island arc/back-arc environment, indiating the two plates should collage in this period（Robinson et al., 1999; Miao et al., 2008；Jian et al., 2010；Chu et al., 2013；Song et al., 2015）; ⑤ The zircon U-Pb age of the Permian clastic deposits in Balin Left Banner showed the final collision and merged time of the two plates should be later than 266 Ma（Zhang et al., 2010）.

(4) Other scholars believe that the collision between the NCC and the SP occurred at the end of the Late Permian, and lasted a long time until the Late Triassic based on the Middle Permian-Middle Triassic syn-collision granite（Zhang et al., 2004；Shi et al., 2022）and the Late Triassic post-orogenic granite（Li et al., 2007；Zhang et al.,2012；Duan et al., 2014；Liu et al., 2017；Chen et al.,2019；Chen et al., 2022b）.

The above debate is resulted from the insufficiently research of the magmatism between the northern margin of the NCC and the XMOB. Magmatism is crucial for tectonic evolution since magmatic rocks are the direct indicator for tectonic evolution inversion. The Chifeng area of Inner Mongolia is located at the junction of the XMOB and the northern margin of the NCC, where is a favorable area to study the attributes, boundaries, collision and merging and magmatic-tectonic evolution of the two tectonic units（Tang，1990）. In recent years, geologists have identified multiple phases of granite assemblages from Early Paleozoic to Mesozoic in the southeastern Inner Mongolia: high-potassium calc-alkaline series rock assemblages formed in an active continental margin environment（Chen et al., 2000，2009；Wu et al., 2011；Liu et al., 2015; Chen et al.,2018, 2019）, potassium feldspar granites and monzogranite with syn-collision properties formed in an compressional environment（Chen et al., 2000，2009；Li et al., 2007；）, and bimodal volcanic rocks and alkaline complex assemblages formed in post-orogenic extensional environment（Zhang et al., 2009a, 2010, 2012）. These granites form in different magmatic-tectonic evolution stages during the closure of the PAO, and are controlled by different geodynamic backgrounds. Some scholars have established the Triassic evolution model of the PAO by systematically studying the Triassic granitic rocks exposed in the Chifeng area(Chen et al.,2019）. However, the evolution process of the PAO in the Permian is still unclear. This paper takes the Permian granite exposed in the Chifeng area of the central northern margin of the NCC as the research object, based on the detailed field geological surveys, petrological, petrography, isotope chronology and systematic petrogeochemical research, the Late Paleozoic magmatic-tectonic evolution of the northern margin of the NCC was discussed, which provided an important scientific basis for temporal and spatial continuous evolution process of PAO.

2. Geological Setting and Sample Descriptions

2.1. Geological Setting

Chifeng area are located between the NCC and XMOB along the central-eastern part of the CAOB, and the specific location is between Solonker-Xar Moron-Changchun-Yanji Suture (SXCYS) and Chifeng-Kaiyuan Fault (Figure 1b). Because of the relatively serious quaternary covering, the bedrock is mainly granitic rock and the strata of different ages（Chen et al., 2018, 2019）. The study area is bounded by Chifeng-Kaiyuan Fault. The north part belongs to CAOB, showing Ordovician, Silurian, Carboniferous and Permian strata(Figure 1b). The south part belongs to NCC, showing Neoarchean metamorphic rocks and Paleoproterozoic Baoyintu Group. During the Mesozoic, the faults occurred in the Paleozoic basement, the study area is transformed into a depression basin. There are continental molasse and coal bearing clastic rock formations in the early and Middle Jurassic, volcanic rocks in the Late Jurassic and coal bearing clastic rock formations in the Cretaceous. In Cenozoic, the differential fluctuation resulted in the basin inheriting and superimposing on the Mesozoic fault basin, and fluvial lacustrine clastic rock deposited and basic volcanic erupted（Chen et al., 2018）.

2.2. Geological and Petrological Characteristics of Permian Granitoid Intrusions

Previous studies on granite in Chifeng area are relatively weak. In recent years, in the process of regional geological survey in Yuanbaoshan, Pingzhuang, Aohan Banner and Beizifu in the east of Chifeng City, the author has disintegrated the plutons in the geology maps of 1:200000 Aohan Banner, Xiawa and Chifeng City. Nine different Permian granitic intrusions were identified in the Chifeng area (Figure 2), including the Mingshan (MS), Jianshanzi (JSZ), Aohan Banner (AH), Daluobogou (DLBG), Xiaodonghuang(XDH), Beizifu(BZF), Shangchaoyanggou(SCYG), Qixieyingzi(QXYZ), and Erdaogou (EDG) plutons. Eight samples and 24 samples were selected from these plutons for geochronological and geochemical analyses, respectively (Figure 2).

Preprints (www.preprints.org) | NOT PEER-REVIEWED | Posted: 21 September 2023 doi:10.20944/preprints202309.1383.v1

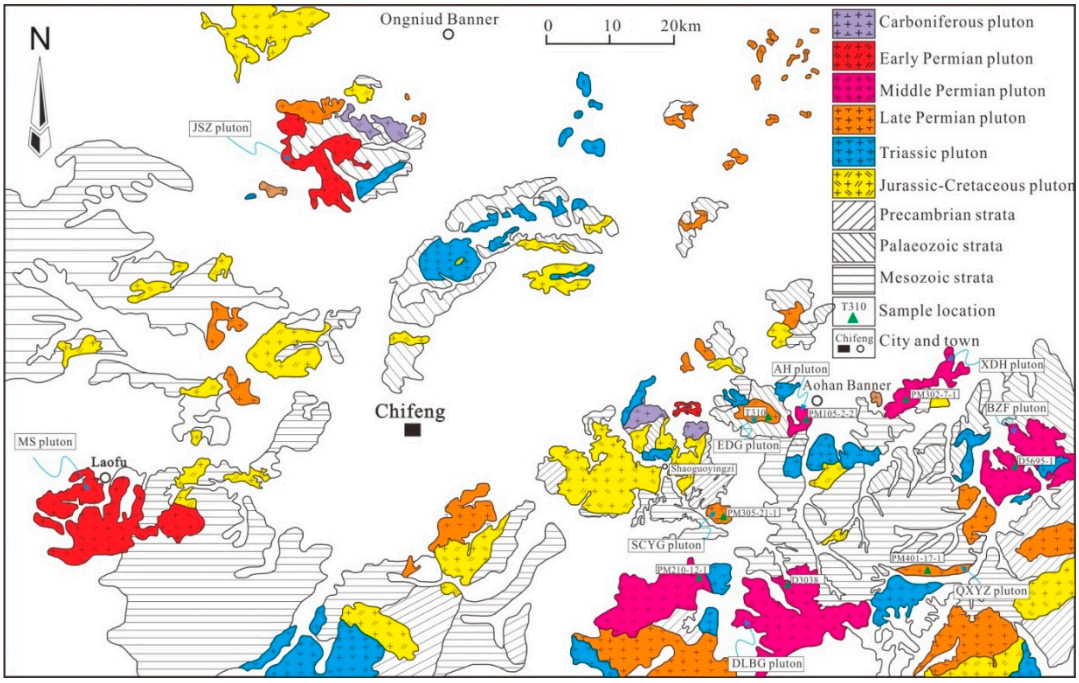

Figure 2. Simplified geological map of the study area in the north margin of the North China Craton showing sample locations, modified after Chen et al., 2019.

There are only two early Permian granitoids in the study area, MS and JSZ plutons. The JSZ pluton, dominated by syenogranite, located at west of the Wutonghua Town of Chifeng City (Figure 2), intrudes Carboniferous Jiujuzi Formation, Permian Sanmianjing and Elitu Formation, and is covered by the volcanic rocks of Baiyingaolao and Hannuoba Formation（Li et al., 2018）. The MS pluton, dominated by porphyritic biotite monzogranite, located at south of the Laofu Town of Chifeng City (Figure 2), intrudes Late Devonian granite, and is covered by the Cretaceous volcanic rocks（Li et al., 2018）. This present cites the previous research results of these two plutons.

The AH pluton, located west of Aohan Banner (Figure 2), is covered by rhyolitic crystal tuff of the Upper Jurassic Manketouebo Formation and andesitic tuff of the Lower Cretaceous Yixian Formation. This granitic pluton is dominated by monzogranites (samples PM105-2-1, PM105-2-2, PM105-2-3, PM105-2-4, PM105-2-4, and PM105-4-1) with fine grained granite texture and massive structure. These samples consist of potassium feldspar (34 wt%), plagioclase (30 wt%), quartz (30 wt%), and biotite (5 wt%), with accessory hematite, limonite, zircon, pyrite, apatite (1 wt%) (Figure 3a).

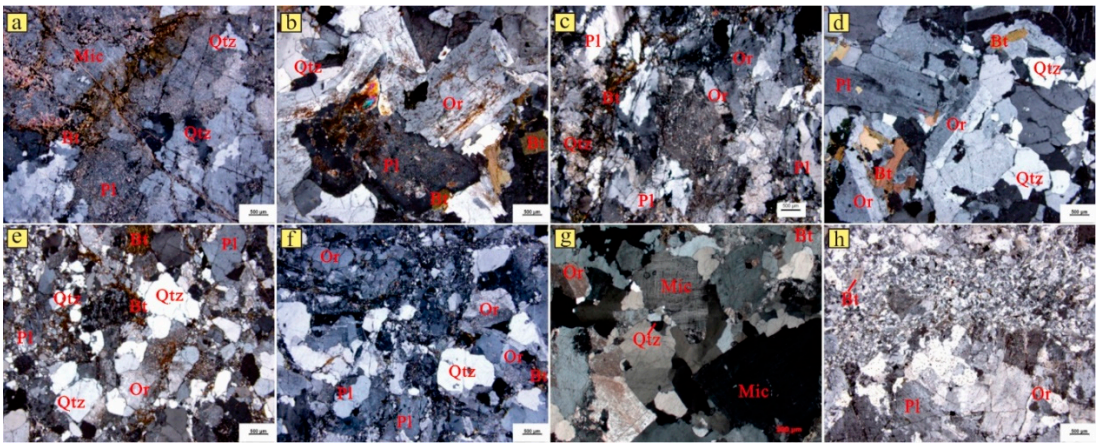

Figure 3. Microphotographs of magmatic rocks from the Chifeng Area (cross-polarized light) showing rock textures. (a)Aohan Banner (AH) pluton(sample PM105-2-2);(b,c)Daluobogou (DLBG)

pluton(sample PM210-12-1, D3038); (c)Xiaodonghuang(XDH) pluton(sample PM302-7-1); (e) Beizifu(BZF) pluton(sample 5695-1); (f)Shangchaoyanggou(SCYG) pluton(sample PM305-21-1); (g) Qixieyingzi(QXYZ) pluton(sample PM410-17-1) and (h)Erdaogou (EDG) pluton (sample T310);.

The DLBG pluton, located 80 km east of Chifeng City (Figure 2), is covered by the volcanic and sedimentary rocks of the Lower Cretaceous Yixian Formation. This pluton is dominated by monzogranites (samples PM210-12-1, D3038-1, D3038-2, D3038-3, D3047-1, D3048-1,and D3049-1) with medium-fine grained texture and massive structure. These samples consist of quartz (25 wt%), plagioclase (28 wt%), potassium feldspar (36 wt%), and biotite (5 wt%), with accessory limonite, zircon and apatite (1 wt%) (Figure 3b, c).

The XDH pluton, located at Xiaodonghuang, Sijianfang, Tengjiawopu in northeast of Fengshou Town Aohan Banner (Figure 2), intrudes the Upper Carboniferous Shizuizi Formation, and is covered by rhyolite and rhyolitic crystal tuff of the Upper Jurassic Manketouebo Formation. This pluton is dominated by porphyritic biotite monzogranite (sample PM302-7-1) with porphyritic texture and massive structure. The matrix is phanerocrystalline with medium-fine grained granite texture. These samples consist of quartz (25 wt%), plagioclase (39wt%), potassium feldspar (30 wt%), and biotite (5 wt%), with accessory zircon, magnetite, sphene (1 wt%) (Figure 3d).

The BZF pluton, located at Beizifu Town 30km east of the Aohan Banner (Figure 2), is intruded by the Mesozoic intrusions. This pluton is dominated by monzogranites (sample 5695-1) with massive structure and medium-fine grained texture. These samples consist of quartz (30 wt%), plagioclase (32wt%), potassium feldspar (34 wt%), and biotite (3 wt%), with accessory apatite, zircon, sphene (1wt%) (Figure 3e).

The SCYG pluton, located at Shangchaoyanggou, Yangjiaogou and Weijiataizi in north of Jianping County (Figure 2), has fault contact with the Cretaceous Yixian Formation and Sunjiawan Formation. This pluton is dominated by monzogranite (sample PM305-21-1) with massive structure and fine grained texture. These samples consist of quartz (25 wt%), plagioclase (25wt%), potassium feldspar (44 wt%), and biotite (5 wt%), with accessory hematite, sphene, zircon (1 wt%) (Figure 3f). The minerals in this monzogranite elongated in NNE direction and showed a certain orientation under influence of Nenjiang- Balihan Fault

The QXYZ pluton, located at Qixieyingzi, Jiangjiagou and Guluyingzi in south of the Aohan Banner (Figure 2), is intruded by Cretaceous monzogranite and coverd by volcanic rocks of the Lower Cretaceous Yixian Formation. This pluton is dominated by syenogranite (samples PM403-2-1, PM403-2-2, PM403-2-3, PM403-2-4, PM403-2-5, PM403-2-6) with massive structure and medium grained texture. These samples consist of potassium feldspar (55 wt%), quartz (25 wt%), plagioclase (15wt%), and biotite (4wt%), with accessory apatite, zircon, sphene (1 wt%) (Figure 3g).

The EDG pluton, located at Erdaogou, Gaojiayaozi and Sanlamayaozi 15km northwest of the Aohan Banner (Figure 2), intrudes the Permian strata (i.e., the Sanmianjing, Elitu, Yujiabeigou Formations), and is covered by rhyolite and andesite from the Lower Cretaceous Yixian Formation. This pluton is dominated by monzogranites (samples T310, PM103-2-1, PM103-2-3, PM103-4-2, PM103-6-1, PM103-6-2, PM103-6-4,) with massive structure and medium grained texture. These samples consist of potassium feldspar (36 wt%), quartz (30 wt%), plagioclase (30wt%), and biotite (3 wt%), with accessory zircon, magnetite, hematite and limonite (1 wt%) (Figure 3h).

3. Analytical Methods

3.1. Sample Preparation

Zircons crystals were separated from whole-rock samples by using conventional heavy liquid and magnetic techniques, and the separates were further purified by hand-picking under a binocular microscope at the Langfang Yuneng Mineral Separation Limited Company, Hebei Province, China. The zircons were selected and embedded in epoxy resin and polished and then imaged using cathodoluminescence (CL) to reveal their internal structures with a scanning electron microscope. CL images of five samples (PM105-2-2、D3038、PM302-7-1、PM401-17-1、T310) were obtained at the

Zhongnan Mineral Supervision and Testing Center of the Ministry of Land and Resources, and the others(PM210-12-1、PM305-21-1、D5659-1) at the electron microprobe Laboratory of the Institute of Geology and Geophysics, Chinese Academy of Sciences.

3.2. Zircon LA-ICP-MS U-Pb Isotope Dating

U-Pb zircon ages for the Permian granites in the Chifeng area were obtained using an Agilent 7500a inductively coupled plasma-mass spectrometry (ICP-MS) instrument equipped with a 193 nm ArF Excimer laser-ablation (LA) system. The spot size was 36 μm for the analyses, with an energy density of 8.5 J/cm^2 and a repetition rate of 10 Hz. Helium was used as the carrier gas to transport the ablated material from the standard LA cell. Zircon 91500 was used as the external standard for age calibration, and standard silicate NIST 610 glass was used to calibrate content calculations (Wiedenbeck et al., 2007). Zircon standards TEMORA (16 ± 5 Ma) and QH (160 ± 1 Ma) were also used as secondary standards to monitor any deviation of age measurement. Isotopic ratios and element contents were calculated using the Glitter software program. The age calculation and concordia plots were obtained using Isoplot (ver 3.0) (Ludwig, 2003). Common Pb was corrected using the method of Andersen (2002). Analyses of five samples (PM105-2-2、D3038、PM302-7-1、PM401-17-1、T310) were conducted at the Zhongnan Mineral Supervision and Testing Center of the Ministry of Land and Resources, and the others(PM210-12-1、PM305-21-1、D5659-1) at the Geologic Laboratory Center, China University of Geosciences (Beijing, China). The analytical results are listed in Table S1.

3.3. Major- and Trace-Element Analyses

Major-, trace-, and rare-earth-element (REE) analyses for 24 samples were performed at the Northeast China Supervision and Inspection Center of Mineral Resources, Ministry of Land and Resources, Shenyang, China. Samples were crushed and ground to 200 mesh in an agate mill after petrographic examination and removal of altered rock surfaces. Whole-rock major-element contents were determined by X-ray fluorescence spectrometry (XRF), yielding analytical precisions of better than 2%. Trace-element and REE contents were determined by ICP-MS, and yielding analytical precisions of better than 5% for elements with contents of >10 ppm, better than 8% for elements with contents of <10 ppm, and 10% for the transition metals. Details of the techniques used for major- and trace-element determinations are described by Li et al., (2005). . The results are listed in Table S2.

4. Analytical Results

4.1. Zircon U-Pb Ages

4.1.1. Early Middle Permian

Sample PM210-12-1 is a monzogranite with fine-grainted collected from DLBG pluton of Machang area. Zircons within this sample are generally colorless, transparent, and mostly subhedral to euhedral columnar in shape. They have length to width ratios of 3:2 to 4:1. In the cathodoluminescence (CL) images (Figure 4), most grains display fine-scale oscillatory growth zoning and clearly internal structure. The zoning, combined with Th/U ratios of 0.42-1.57 (Table S1), indicates a magmatic origin (Belousova, et al., 2002; Hoskin and Ireland., 2000). Twenty-four isotopic analyses were conducted on 24 zircons grains from this sample. Most of the analyses are concordant and define a weighted mean $^{206}Pb/^{238}U$ age of 269±1 Ma (MSDW=0.90) (Figure 5a), which is interpreted as the crystallization age of the monzogranite.

Preprints (www.preprints.org) | NOT PEER-REVIEWED | Posted: 21 September 2023 doi:10.20944/preprints202309.1383.v1

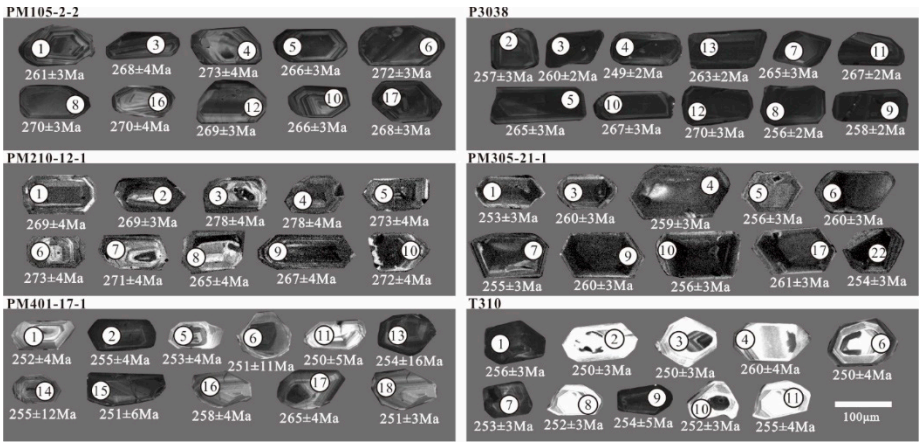

Figure 4. Cathodoluminescence (CL) images of selected zircon grains from Permian granites in this study.

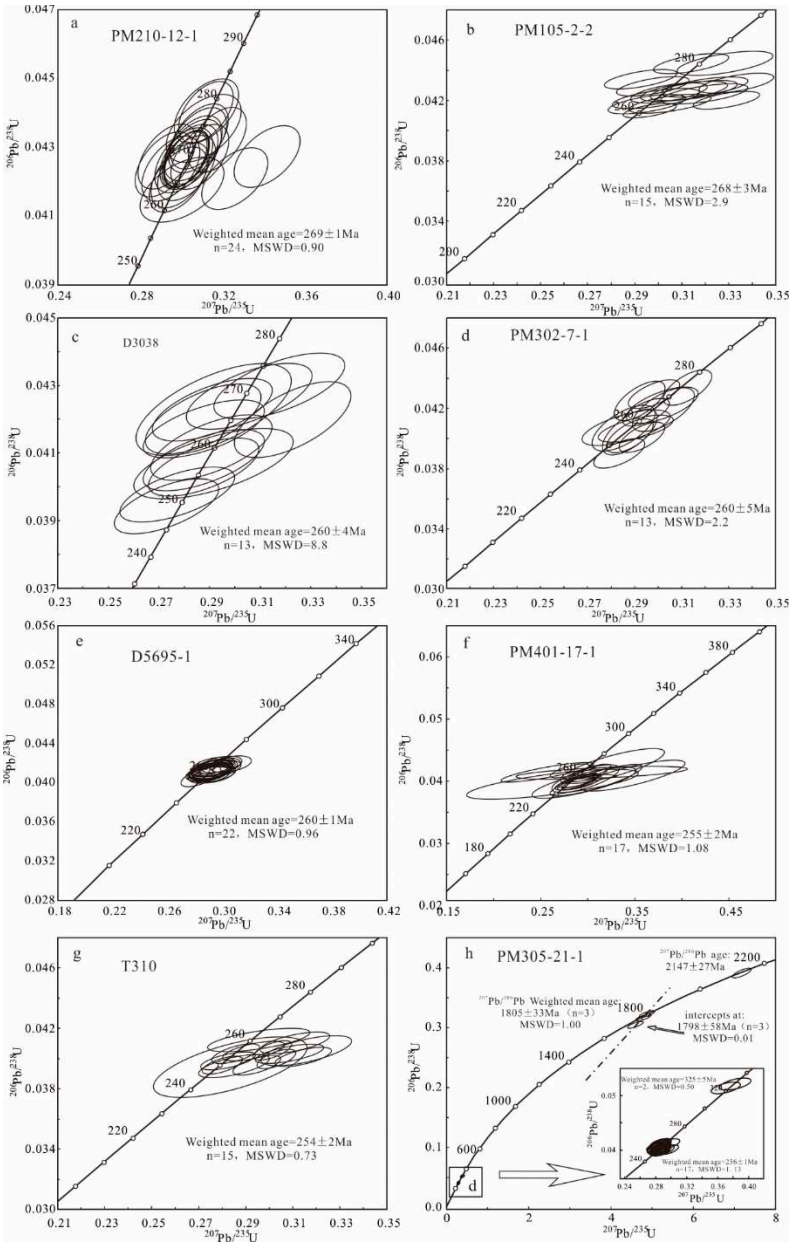

Figure 5. Zircon $^{207}Pb/^{235}U$-$^{206}Pb/^{238}U$ concordia diagrams of Permian granites samples from this study.

Sample PM105-2-2, a fine-grained biotite monzogranite, was collected from AH pluton. Zircons from this sample are translucent and euhedral to subhedral or form short prisms to long columns in shape. They have length to width rations of 2:1 to 3:1. CL imaging reveals that most zircons are bright with fine-scale oscillatory growth zoning (Figure 4), indicating a magmatic origin (Belousova, et al., 2002; Hoskin and Ireland., 2000). A total of 18 analyses were made on 18 zircons, and they have a higher Th/U ratios (0.43-0.88) (Table S1). In the concordia diagram(Figure 5b), the three analysis points did not participate in the diagram because of the low compatibility (less than 90%). The other 15 analysis points are ploted on or near the concordia line and have good concordant. The concordant zircon data give a weighted mean $^{206}Pb/^{238}U$ age of 268±3 Ma (MSDW=2.90), interpreted as the emplacement age of the sample.

4.1.2. Late Middle Permian

Sample D3038 is a medium-grained monzogranite from the DLBG pluton near the Luofugou area. The zircon grains from the sample are mostly euhedral elongate prisms with oscillatory zoning. They have length to width ratios of 2:1 to 4:1 and Th/U ratios of 0.52 to 1.31(Figure 4), indicative of a magmatic origin (Belousova, et al., 2002; Hoskin and Ireland., 2000). A total of 15 analyses on 15 zircon grains were conducted. All but two of the analyses are concordant and yield a weighted mean $^{206}Pb/^{238}U$ age of 260±4 Ma (MSDW=8.8) (Figure 5c), which can be regarded as the emplacement age the monzogranite.

Sample PM302-7-1, a porphyry monzogranite, was collected from the XDH pluton of Fengshou village, Aohan Banner. Zircon grains from this sample are prismatic and stubby in shape, and Th/U ratios mostly cluster around 0.43-1.38 (Table S1). Twenty-five analyses were made on 25 zircons. Ten analyses were excluded because of high discordancy. The remaining 15 analyses spots yield a weighted mean $^{206}Pb/^{238}U$ age of 260±1 Ma (MSDW=0.96) (Figure 5d), is considered to represent the crystallization age of porphyry monzogranite.

Sample D5695-1, a medium-grained monzogranite, was collected from the BZF pluton. Sample D5695-1 contains zircons that are generally colorless, transparent, and euhedral in shape. In CL images, most of them display fine-scale ocillatory zoning, with high Th/U ratios of 0.29-1.35, indicating a magmatic origin (Belousova, et al., 2002; Hoskin and Ireland., 2000). A total of 25 spots were analysed on 25 zircons from this sample. Three analyses were excluded because of high discordancy. The remaining 22 spots are concordant, with the eceptions exhibiting a loss of common Pb. The concordant zircons data give a weighted mean $^{206}Pb/^{238}U$ age of 260±1 Ma (MSDW = 0.96) (Figure 5e), interpreted as the emplacement age of the sample.

4.1.3. Late Permian

Sample PM401-17-1, a medium grained syenogranite, was collected from the QXYZ pluton. Zircons within sample PM401-17-1 are generally euheral and prismatic with length to width ratios of 2:1-4:1. They show variable degrees of oscillatory zoning visible during CL imaging(Figure 4), and have Th/U ratios of 0.43-2.83 (Table S1), characteristic of magmatic zircons of acid rocks (Belousova, et al., 2002; Hoskin and Ireland., 2000). Excluding three discordant data point probably caused by lead loss, the others 17 analyses spots yield a weighted mean $^{206}Pb/^{238}U$ age of 255±2 Ma (MSDW=1.08) (Figure 5f). We interpret this age to be the crystallization age of the syenogranite.

Sample T310, a medium grained monzogranite, was collected from the EDG pluton. Zircon grains within this sample are generally colorless, transparent, and short columnar in shape with maximum length to width ratio of 2:1. CL imaging reveals that most grains have fine oscillatory zones (Figure 4). These properties, together with their relatively high Th/U ratios (0.43-2.97) (Table S1), suggest the zircons are magmatic origin (Belousova, et al., 2002; Hoskin and Ireland., 2000). A total of 15 analyses are consistent and define a weighted mean $^{206}Pb/^{238}U$ age of 254±2 Ma (MSDW=0.73) (Figure 5g), which is interpreted as the time of crystallization of the monzogranite.

Sample PM305-21-1 is a monzogranite collected from the SCYG pluton. Sample PM305-21-1 contains zircons that are generally euhedral and prismatic with length to width ratios of 2:1 to 3:1. In the CL images, most grains display fine-scale oscillatory growth zoning(Figure 4), with high Th/U

Preprints (www.preprints.org) | NOT PEER-REVIEWED | Posted: 21 September 2023 doi:10.20944/preprints202309.1383.v1

values of (0.28-1.92) (Table S1). A total of 25 spots were analysed on 25 zircons from this sample. Two analyses were excluded beacause of high discordancy, the remaining 23 analysis points are ploted on and near the concordia line, and give four groups of ages(Figure 5h). The first group consists of one analyse (No. 16) with $^{207}Pb/^{206}Pb$ age of 2147±27 Ma, representing one magmatic event. The second group consists of three analyses (No. 11, 18, 20) and yield a weighted mean $^{207}Pb/^{206}Pb$ age of 1805±33Ma, which is consistent with their upper intercept age of 1798±58 Ma in error range, representing a magmatic activity. The third group consists of two analyses (No. 14, 15) and yield a weighted mean $^{206}Pb/^{238}U$ age of 352±5 Ma (MSDW=0.50) (Figure 5h). The fourth group consists of 17 analyses and yield a weighted mean $^{206}Pb/^{238}U$ age of 256±1 Ma (MSDW=1.13). The youngest age of 256±1Ma is interpreted to be the emplacement age of the monzogranite from the SCYG pluton, whereas the other three ages (ca. ~2147, ~1805 and ~352 Ma) respresent the crystallization ages of captured zircon entrained by the granitic magma.

4.2. Major and Trace Element Geochemistry

4.2.1. Early Middle Permian Monzogranite

The monzogranites are high in SiO_2 (72.00-73.37 wt%), K_2O (4.32-4.70 wt%) and (Na_2O+K_2O)(14.17-14.62 wt%) with Na_2O/K_2O ratios of 0.88-1.01, but low in TiO_2 (0.12-0.20 wt%), MnO (0.02-0.03 wt%), MgO (0.04-0.15 wt%) and P_2O_5 (0.04-0.07 wt%) (Table S2). They are classified in the alkalic series (Irvine and Baragar, 1971), and assigned to the high-K cal-calkaline igneous rocks (Figure 6a, Peccerillo and Tayor, 1976). Their A/CNK (molar $Al_2O_3/(CaO+Na_2O+K_2O)$) values range from 1.08 to 1.23, indicative of weakly peraluminous granites (Figure 6b, Maniar and Piccoli, 1989). The total rare earth elements (REEs) range from 143.96 to 156.29×10^{-6} (except for one data lower than 66.45 ×10^{-6}). In the chondrite-normalized REE diagram(Figure 7a), the monzogranite samples have slightly enriched LREEs but flat HREEs pattern, with $(La/Yb)_N$ and ΣLREE/ΣHREE (Total light rare earth elements versus total heavy rare earth elements) ratios of 3.54-19.62 and 5.29-10.06 and moderate negative Eu anomalies (Eu/Eu* = 0.42-0.57). In the primitive-mantle (PM) normalized trace element diagram(Figure 7b), all samples show negative Sr, P, and Ti anomalies, and they are all enriched in Rb, Th, K, La, Zr, and Hf.

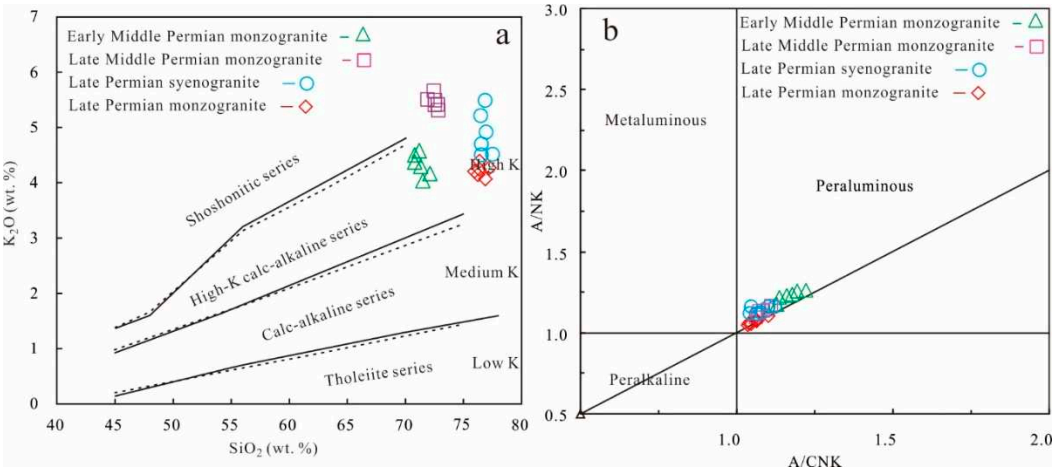

Figure 6. (a) K_2O versus SiO_2 diagram for intrusive rocks. Normalization values are from Rickwood (1989); (b) A/NK (molar/molar) versus A/CNK (molar/molar) diagram for these rocks. Normalization values are from Rickwood (1989).

Preprints (www.preprints.org) | NOT PEER-REVIEWED | Posted: 21 September 2023 doi:10.20944/preprints202309.1383.v1

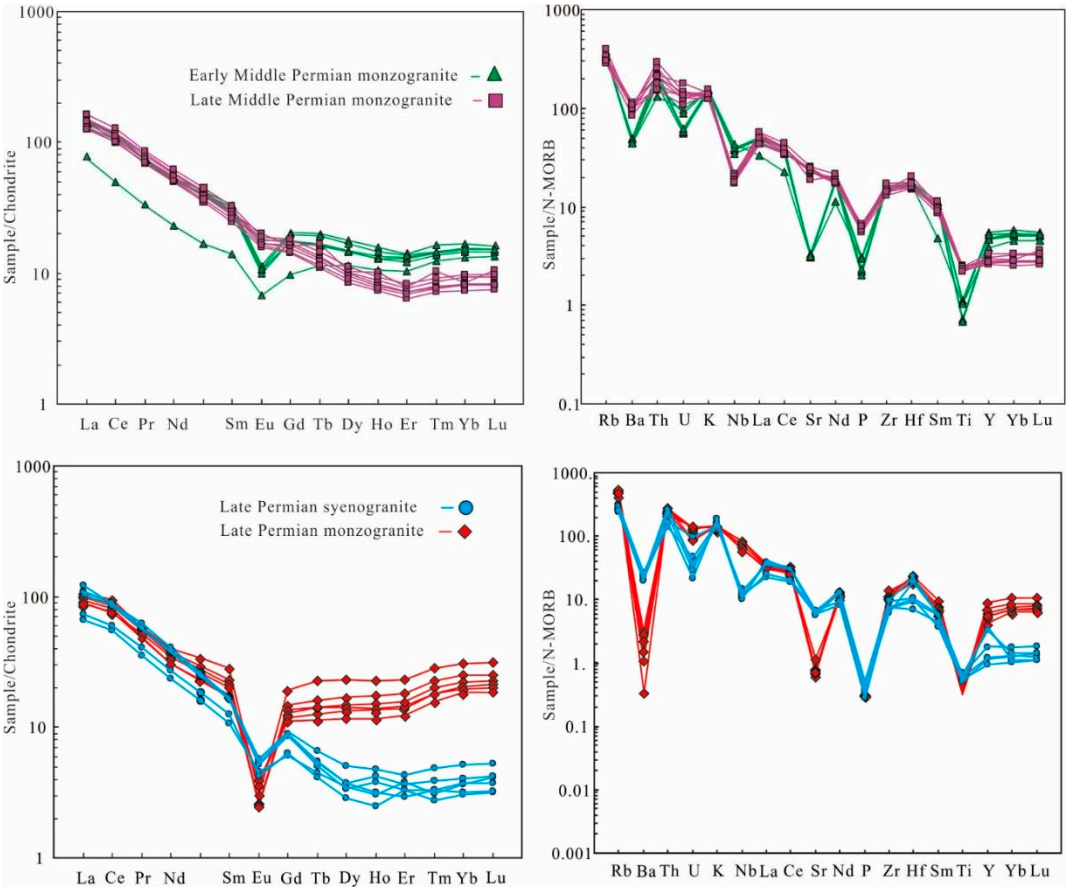

Figure 7. Chondrite-normalized rare earth element patterns and Primitive mantle normalized trace element spider diagram for these Permian granitic rocks. The values of chondrite and primitive mantle are from Sun and McDonough (1989).

4.2.2. Late Middle Permian Monzogranite

All of the monzogranite samples are alkalic-rich and silica-rich high-K calc-alkaline igneous rocks (Figure 6a) (Peccerillo and Taylor, 1976). Whole rock analyses yield SiO_2 = 73.40-74.11 wt%, Na_2O/K_2O ratios = 0.65-070, and total Na_2O+K_2O = 9.30-9.76. The samples are low in TiO_2 = 0.16-0.18 wt%, MnO = 0.03-0.04 wt%, MgO = 0.20 wt%, and P_2O_5 = 0.03 wt% (Table S2). They are classified as potassium basalt series and weakly peraluminous granites owing to their A/CNK, K_2O and Al_2O_3 values of 1.07-1.11, 5.47-5.80 wt% and 13.93-14.21 wt%, respectively (Figure 6b, Maniar and Piccoli, 1989). The total REEs range from 272.5 to 340.64 $\times 10^{-6}$. The chondrite-normalized REE diagram invariaby show an relative enrichment in LREE and moderate to significant negative Eu anomalies, with $(La/Yb)_N$, ΣLREE/ΣHREE, and Eu/Eu* ratios of 19.58-26.88, 18.36-20.38, and 0.31-0.41, respectively(Figure 7a). Furthermore, in the PM-normalized trace element diagram(Figure 7b), the rocks are enriched in large ion lithophile elements (LILEs)(e.g., Rb, Th, K, La and Ce) and depleted in high field strength elements (HFSEs) (e.g., P, Ti and Sr).

4.2.3. Late Permian Monzogranite and Syenograntie

The Late Permian monzogranite have SiO_2= 76.29-77.30 wt% and contain Al_2O_3 of 12.75-12.93 wt%, TiO_2 of 0.06-0.07 wt%, MnO of 0.01-0.08 wt%, MgO of 0.11 wt%, P_2O_5 of 0.01 wt%, and total Na_2O+K_2O of 8.40-8.79 wt%, with Na_2O/K_2O ratios of 0.95-1.09 (Table S2). They are classified as the weakly peraluminous high-K calc-alkaline series on a plot of K_2O against SiO_2 (Figure 6a, Peccerillo and Taylor, 1976), and plot in the peraluminous field in the A/CNK vs. A/NK diagram (Figure 6b, Maniar and Piccoli, 1989). The total REEs range from 101.75 to 128.91 $\times 10^{-6}$. In the chondrite-normalized REE diagram, they are weakly fractionated, with $(La/Yb)_N$ and ΣLREE/ΣHREE ratios of

3.28-5.06 and 4.73-7.25 and strong negative Eu anomalies (Eu/Eu* = 0.13-0.28) (Figure 7c). In the PM-normalized trace element diagram(Figure 7d), they show similar patterns, although there are notable difference in the absolute element concentrations. All samples are enriched in Rb, Th, U, K, Nd, Zr and Hf, but are depleted in Ba, P, Ti and Sr.

The Late Permian syenograntie are high in SiO_2 (76.22-77.58 wt%) and K_2O (4.35-5.62 wt%), but low in Al_2O_3 (12.05-12.63 wt%), TiO_2 (0.09-0.16 wt%), MnO (0.01-0.05 wt%), MgO (0.20-0.56 wt%), and P_2O_5 (0.01-0.02 wt%) contents. They belong to high-K calc-alkaline, and weak peraluminous igneous rocks (Figure 6a, Peccerillo and Taylor, 1976), with total Na_2O+K_2O of 0.49-0.86, Na_2O/K_2O ratios of 0.49-0.86, and A/CNK ratios ranging from 1.05 to 1.16 (Figure 6b, Maniar and Piccoli, 1989). All but two have high in total REEs, the total REEs values range from 107.94 to 215.80×10^{-6}. The chondrite normalized REE diagram show that they are enriched in LREEs, with $(La/Yb)_N$ and ΣLREE/ΣHREE ratios of 18.05-32.16 and 16.77-25.86(Figure 7c). The granites also have weak to moderate negative Eu anomalies (Eu/Eu* = 0.39-0.54). They are enriched in LILEs (e.g., Rb, Th, K, La and Ce) and LREEs (e.g., Nd, Zr and Hf), and depleted in HFSEs (e.g., Ba, P, Ti and Sr) from the PM-normalized trace element diagram(Figure 7d).

5. Discussion

5.1. Permian Magmatism in the Chifeng Area

Previous research on the Permian magmatism in the Chifeng area are relatively limited, only including the granodiorite formed in the Late Permian in Mengguyingzi（Liu et al.,2015）, the diorite hosting granulite (256 ±6Ma) in Chaihuyingzi（Shao et al.,2012）, the gneissic monzogranite in the Liangjin mining area of Jinchanggou (249±1Ma) （Duan et al.,2014）, the Early Permian monzogranite in the Mingshan pluton and the syenite in the Jianshanzi pluton (284.4 ±7.9Ma, 294.7±8.5Ma) （Li et al.,2018）. The coeval volcanic rocks include the hornblende andesite of the Permian Elitu Formation that exposed in the Mingshan uplift belt in the west of Chifeng (273Ma). Based on available data, combining with data in this study, the Permian granitic chronology framework of the Chifeng area was established(Table 1).

Table 1. Geochronological data for the Permian granitic rocks in Chifeng area.

Order	Sample	Plunton	Lithology	Age(Ma)	Method	References
1	14CH10	Jianshanzi	Monzogranite	294	LA-ICPMS	Li et al., 2018
2	14CH24	Mingshan	Granodiorite	284	LA-ICPMS	Li et al., 2018
3		Majiadi	Granite	274	LA-ICPMS	Regional geological survey
4	PM210-12-1	Daluobogou	Monzogranite	269	LA-ICPMS	This study
5	PM105-2-2	Aohan banner	Monzogranite	268	LA-ICPMS	This study
6	D3038	Daluobogou	Monzogranite	260	LA-ICPMS	This study
7	PM302-7-1	Xiaodonghuang	Monzogranite	260	LA-ICPMS	This study
8	D5695-1	Beizifu	Monzogranite	260	LA-ICPMS	This study
9		Sidaogou	Syenogranite	267	LA-ICPMS	Regional geological survey
10		Jianshanzi	Monzogranite	263	LA-ICPMS	Regional geological survey
11	PM305-21-1	Shangchaoyanggou	Granodiorite	256	LA-ICPMS	This study
12	PM401-17-1	Qixieyingzi	Syenogranite	255	LA-ICPMS	This study
13		Zhaojiawopu	Diorite	253	LA-ICPMS	Regional geological survey
14	T310	Erdaohou	Monzogranite	253	LA-ICPMS	This study
15	T101	Mengguyingzi	Granodiorite	251	LA-ICPMS	Chen et al.,(2019)
16	D2711-1	Xiaxinjing	Monzogranite	250	LA-ICPMS	Chen et al.,(2019)
17	PM210-6-1	Daluobogou	Monzogranite	247	LA-ICPMS	Chen et al.,(2019)
18	CH2	Chaihulanzi	Diorite	260	SHRIMP	Shao et al.,2012
19	DJ10-18	Shuangjingzi	Granite	278	LA-ICPMS	Jiang et al.,2014

 doi:10.20944/preprints202309.1383.v1

20	PM003-1	Mengguyingzi	Granodiorite	253	LA-ICPMS	Liu et al.,2015
21		Dayingzi	Syenogranite	268	LA-ICPMS	Xi et al.,2015
22	XG01	Jinchanggouliang	Monzogranite	250	LA-ICPMS	Duan et al.,2014

5.1.1. Early Permian（294～284Ma）

The magmatic activities are intense in the Permian in the northern margin of the NCC. But these magmatic activities are mainly concentrated in the central region of Inner Mongolia, and are not commonly seen in the Chifeng area. The Early Permian granite studied in this paper includes the syenite in the Jianshanzi pluton (294 Ma) and the monzogranite in the Mingshan pluton (284 Ma), indicating the Early Permian granite of the Chifeng area formed during 294～284Ma（Li et al.,2018）.

5.1.2. Middle Permian（269～260Ma）

Late Paleozoic magmatic rocks are lineshape widespread in the study area and its adjacent area. Among them, the Middle Permian magmatic rocks are the most widely distributed. They are exposed on the northern margin of the NCC and the **XMOB**. In the Chifeng area, the syenite (269 Ma) and monzogranite (260 Ma) in the DLBG pluton, the fine-grained monzogranite of Aohan Banner (268 Ma), the porphyritic medium-coarse monzogranite of XDH (260Ma) and the medium-grained monzogranite of BZF (260Ma) are identified. The syenite at the margin of the Dayingzi pluton in the northwestern Chifeng has an age of 268 Ma（Xi et al.,2015）. The zircon U-Pb dating results show that the Middle Permian intrusive rocks formed between 269 and 260 Ma, indicating magmatism took place in Middle Permian in the Chifeng area.

5.1.3. Late Permian～Early Triassic（256～248Ma）

The Late Permian-Early Triassic granitic magmatism in the research area occurs frequently in the same tectonic background, and the magmatism of the Early Triassic inherits that of the Late Permian（Zhang et al., 2009a, 2010）. The Late Permian granitic rocks identified in the research area include the weak gneissic monzogranite of the upper SCYG pluton (256Ma), the medium-grained syenite of the QXYZ pluton (255Ma), and the medium-grained monzogranite of the EDG pluton (253Ma). There are also other magmatic activities, such as the diorite hosting the granulite in the Chaihuyingzi (256±6Ma) （Shao et al.,2012）, the fine-grained granodiorite of the Mengguyingzi (252±2Ma) （Liu et al.,2015）, the gneissic monzonite of the Liangjin mining area of the Jinchanggou (249±1Ma) （Duan et al.,2014）, the fine-grained granodiorite in the Mongoliayingzi pluton (251Ma), the medium-grain monzonite in the Xiaxinjing pluton (250Ma) and the medium-grained syenite in the DLBG pluton (247Ma) （Chen et al., 2019）. These granintic rocks further proves magmatic events are intense. The zircon U-Pb ages of these granitic intrusions range from 256 to 247 Ma, indicating the most intense magmatism in the Late Permian-Early Triassic.

5.2. Genetic Types of the Middle-Late Permian Granitic Rocks from the Chifeng Area

5.2.1. Middle Permian Monzogranite

The early Middle Permian monzogranite (269Ma) is alkali-rich and high-potassium calc-alkaline rock, rich in Si and aluminum on the whole, with high total alkali content w (Na_2O+K_2O) and Na_2O/K_2O of 0.88～1.01. A/CNK value is between 1.08 and 1.23, indicating peraluminous. ∑REE is low, which is the average level of continental crust. Eu is moderately depleted. The fine-grained monzogranite belongs to aluminum-saturated, high-potassium calc-alkaline rocks. All the Middle Permian granite falls in the range of classic island arc rocks in the $(La/Yb)_N$ -Yb_N diagram and Y-Sr/Y diagram (Figure 8). By comparing the trace element ratio of fine-grained monzogranite to that of continental crust average value and differentiated granite, it is concluded that the monzogranite of this phase is I-type granite.

Preprints (www.preprints.org) | NOT PEER-REVIEWED | Posted: 21 September 2023 doi:10.20944/preprints202309.1383.v1

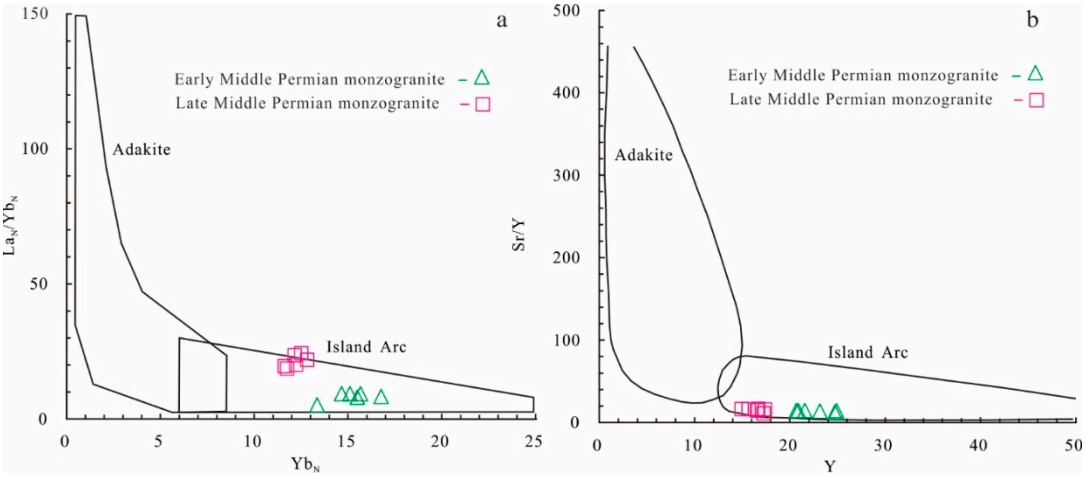

Figure 8. (a) La_N/Yb_N versus Yb_N; (b) Sr/Y versus Y diagram of the Middle Permian granites in Aohan area, modified after Whalen et al. (1987).

The late Middle Permian monzogranite (260Ma) is alkali-rich, high-potassium, calcium-alkaline rock, rich in Si, with medium Al, high total alkali content w (Na_2O+K_2O) and Na_2O/K_2O of 0.65～0.70. ∑REE is very high, much higher than the average level of continental crust. Eu is moderately depleted. A/CNK value is between 1.07 and 1.11, indicating slightly peraluminous. The medium-grained monzogranite belongs to slightly aluminum-saturated, alkali rich, high-potassium calc-alkaline rocks. It falls in the range of classic island arc rocks in the $(La/Yb)_N$ -Yb_N diagram and Y-Sr/Y diagram (Figure 8). By comparing the trace element ratio of fine-grained monzogranite to that of continental crust average value and differentiated granite, it is concluded that the Middle Permain medium-grained monzogranite in the DLBG pluton is I-type granite.

5.2.2. Genesis of the Late Permian Granite

Lithogeochemistry characteristics show that the Late Permian monzogranite is alkali-rich, high-potassium, calc-alkaline rocks, rich in Si and poor in Al, with w (Na_2O+K_2O) of 8.40-8.86％ and Na_2O/K_2O of 0.94-1.19. A/CNK value is 0.95～1.05, indicating moderately peraluminous. NK/A value is 0.89-94 (>0.85). ∑REE is closed to the average level of continental crust. Eu is slightly depleted. The monzogranite is alkali rich, medium-aluminum high-potassium calc-alkaline rocks. The trace elements have similar characteristics to those of A-type granite（Zhang et al.,2012）: The light and heavy rare earth elements are obviously fractionated, with strong negative Europium anomalies. The rare earth element distribution pattern is “swallow”. High field strength elements, Nb, Zr and Hf are high in content, but Sr and Ba element is low, showing the characteristics of A-type granite. In the 10000Ga/Al-Zr, 10000Ga/Al-Nb, and 10000Ga/Al-Na_2O+K_2O diagram (Figure 9a,b,c) of Late Permian intrusive rocks, the monzogranite falls in the range of A-type granite. The (Zr+Nb+Ce+Y) content of the monzogranite is not high (288.49×10^{-6}～354.33×10^{-6}, less than 350×10^{-6} Zhang et al.,2012), which is slightly lower than the (Zr+Nb+Ce+Y) value of A-type granite (usually greater than 350×10^{-6}), but exceptions did exist（Chappell and White，1992）. It falls in the range of A-type granite in the （Zr+Nb+Ce+Y）-（K_2O+Na_2O）/CaO diagram (Figure 9d). Zhang Qi et al. (2012) considered that A-type granite should be distinguished based on the comprehensive analyses of (Zr+Nb+Ce+Y) diagram, rare earth element and trace element diagram rather than only based on (Zr+Nb+Ce+Y) diagram （Zhang et al.,2012）. The most important geochemical characteristics of A-type granite are rich in SiO_2 (usually> 70%, mostly> 75%), rich in K_2O (4%- 6% or higher), depleted in Al_2O_3 (content of 12%-13%), Sr, Ba, Eu, Ti and P, swallow REE pattern and obviously negative Europium anomaly（Zhang et al.,2012）. The monzogranite has a SiO_2 content of 76.32%-77.20%, K_2O content of 4.15% -4.47%, and Al_2O_3 content of 12.77% -12.93%, showing negative anomalies of Sr, Ba, Ti and P. The monzogranite has rare earth element distribution pattern of “swallow” tetrad effect and obviously negative Europium anomaly, which is the same as the A-type granite distributed in northeastern China（Wu et al.,2002）. A-type granite generally formed in high temperature environment. With the

 doi:10.20944/preprints202309.1383.v1

Zr saturation temperature of 807-828℃, the monzogranite in the EDG pluton is not high temperature granite. However, experimental petrology shows that when the pressure is less than 0.5 GPa and the water content is 1%-6%, the partial melting temperature of A-type granite can be reduced to 800-830°C（Clemens et al., 1986；Klimm et al ., 2003）, or even lower（Anderson, 1983；Scaillet and Macdonald , 2001 , 2003）. In summary, it is concluded that the Late Permian monzonitic granite is A-type granite.

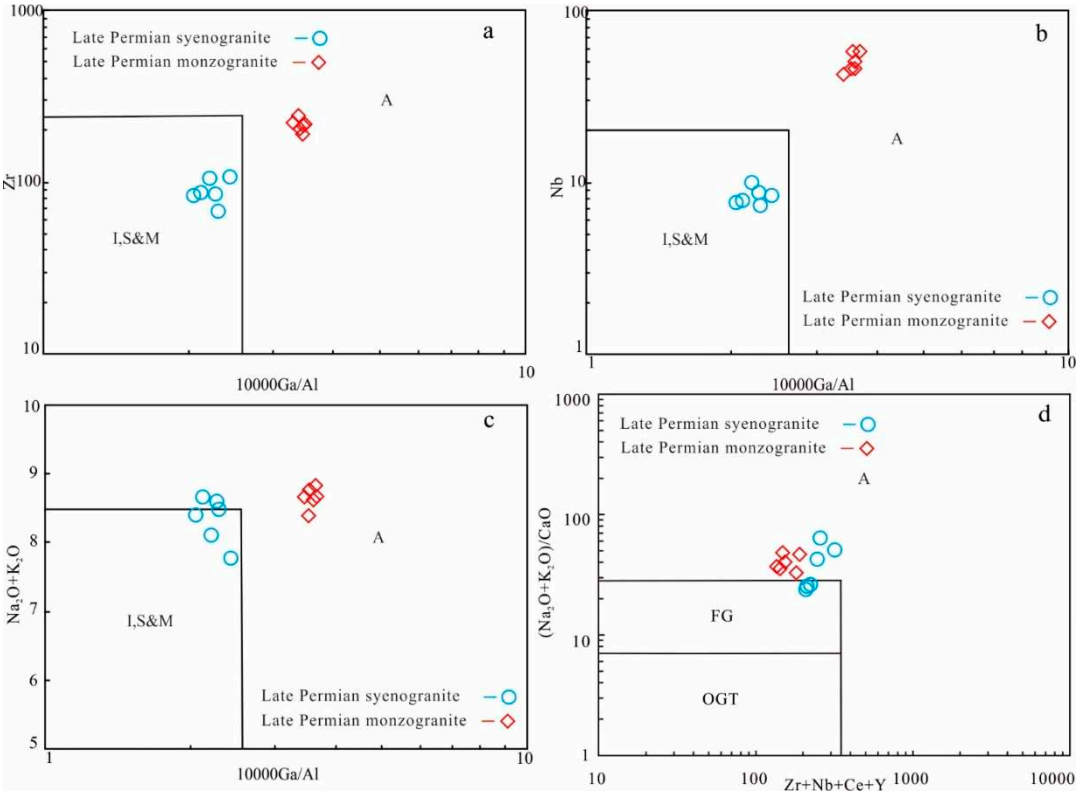

Figure 9. Diagram of 10000Ga/Al vs. Zr, Nb, Na_2O+K_2O(a,b,c), and (Zr+Nb+Ce+Y) vs. (Na_2O+K_2O/CaO) (d) for the Late Permian granitic intrusions（Collins W J, et al.,1982）. A, A-type granite; FG, highly fractionated I-type granite; I,S&M,OGT, unfractionated I, S and M-type granite.

Syenogranite is high potassium calc-alkaline rock, rich in Si, depleted in Al, with high total alkali content w (Na_2O+K_2O) of 8.09-8.74 % and Na_2O/K_2O of 0.49-0.86. A/CNK value is 1.05-1.16, indicating slightly peraluminum. NK/A value is 0.85- 91 (>0.85). Content or the ∑REE is closed to the crust average level. Eu is moderately negative anomaly. Syenogranite does not fall in the range of A-type granite in the 10000Ga/Al-Zr and 10000Ga/Al-Nb diagram. Syenogranite shows the characteristics of A-type granite, with SiO_2 content of 76.22%-77.58%, K_2O content of 4.35%-4.87%, Al_2O_3 content of 12.05% -12.56% and negative anomalies of Sr, Ba, Eu, Ti, and P（Zhang et al.,2012）. The samples fall in the transitional range of I, S and A-type granite in the 10000Ga/Al-Na_2O+K_2O diagram (Figure 9a,b,c), but fall in the range of A-type granite in the (Zr+Nb+Ce+Y)-(K_2O+Na_2O)/CaO diagram (Figure 9d). In the standardized diagram of rare earth element chondrites(Figure 7c), the syenogranite does not show the “swallow” tetrad effect and obviously negative Europium anomaly, which is inconsistent with the characteristics of A-type granite（Wu et al.,2002）, combined with its relatively low content of (Zr+Nb+Ce+Y) (132.44～185.68μg/g), it is considered that the syenogranite belongs to I-type granite rather than A-type granite.

5.2.3. Petrogenesis of High-K I-type Granitic Rocks of the Permian

As discussed above， both the Middle Permian monzogranite and the Late Permian syenogranite in the Chifeng area belong to high-K calc-alkaline I-type granites，and the origins of this kind of granites are still debated (e.g., Roberts and Clemens, 1993; Liegeois et al., 1998). Some

 doi:10.20944/preprints202309.1383.v1

scholars believed the model of fractional crystallization and crustal assimilation of mantle-derived basaltic magma (e.g., DePaolo, 1981; Moghazi, 2003), a number of scholars insisted the model of mixing of crust-derived and mantle-derived magmas (e.g., Dickinson, 1975; Yang et al., 2006; Yang et al., 2015; Clemens et al., 2009), and the others researchers had attributed the model of partial melting of hydrous medium- to high-K andesitic to basaltic meta-igneous rocks under crustal conditions (e.g., Roberts and Clemens, 1993; Sisson et al., 2005; Topuz et al., 2010).

The Permian granitic rocks belong to the classic high-K I-type granites. And these rocks have high silica and alkali contents and low MgO, TFe_2O_3, CaO, and transition-element contents, as well as positive Th, Zr, and Hf anomalies and negative Nb, Ta, P, and Ti anomalies in a primitive mantle-normalized diagram. These different characteristics indicate that the primary magma of these rocks originated from the partial melting of continental crust, and may be produced by the chemical differentiation of arc-derived magma (Hofmann, 1988; Yu et al., 2013). The moderate-strong negative Eu anomalies of the granite sample indicate that plagioclase is retained in the residue of the source or fractionated during magma evolution (Springer and Seck, 1997). These geochemical characteristics indicate that these high-K I-type granites of Permian were formed by partial melting of lower crustal source under a relatively low-pressure condition.

5.3. Tectonic Implications and Geological Significance

5.3.1. Tectonic Setting

5.3.1.1. Tectonic Setting of the Middle Permian Monzogranite

In recent years, some scholars have speculated that the PAO was closed in the Early Permian based on a late Early Permian-Middle Permian alkaline-peralkaline intrusion (276Ma～259Ma) distributed on the northern margin of the NCC, which indicating a post-collision environment in the Middle Permian（Zhang et al., 2007；Li et al., 2007；Wang.,2014；）. All the intrusions studied by these scholars are located in the Jining area in the middle section of the northern margin of the NCC. But the characteristics of the rock assemblages in the Middle Permian in the Changchun-Yanji area of the eastern section of the northern margin of the NCC show an active continental margin（Yu et al.,2013）, and the widespread diorite, tonalite , and granodiorite indicate the active continental marginal environment lasted until the Late Permian（Zhang et al., 2004；Cao et al., 2011）. So the eastern section of the northern margin of the NCC was still under the subduction background of the PAO in the Middle Permian（Cao et al., 2011）. What is the tectonic background of the Chifeng area in the middle during the Middle Permian?

The Middle Permian granitic magma covers a large area in the Chifeng and mainly dominated by monzogranite. Geochemical characteristics show that the monzogranite is the I-type granite originating from the lower crust. In the Y-Nb diagram, all the samples fall in the volcanic arc and syn-collision area(Figure 10a). But they fall in the transitional range between the volcanic arc and the syn-collision, deviated to the syn-collision area in the Yb+Ta vs. Rb diagram (Figure 10b). In the R1-R2 structural environment discriminate diagram, they belong to the syn-collision granite(Figure 11). Compared to the tectonic environment discriminant ratio of the orogenic granite proposed by Miniar (1999), the monzogranite has similar characteristics with continental collision granite (CCG). Therefore, the Middle Permian monzogranite in the Chifeng area formed in a syn-collision environment.

Preprints (www.preprints.org) | NOT PEER-REVIEWED | Posted: 21 September 2023 doi:10.20944/preprints202309.1383.v1

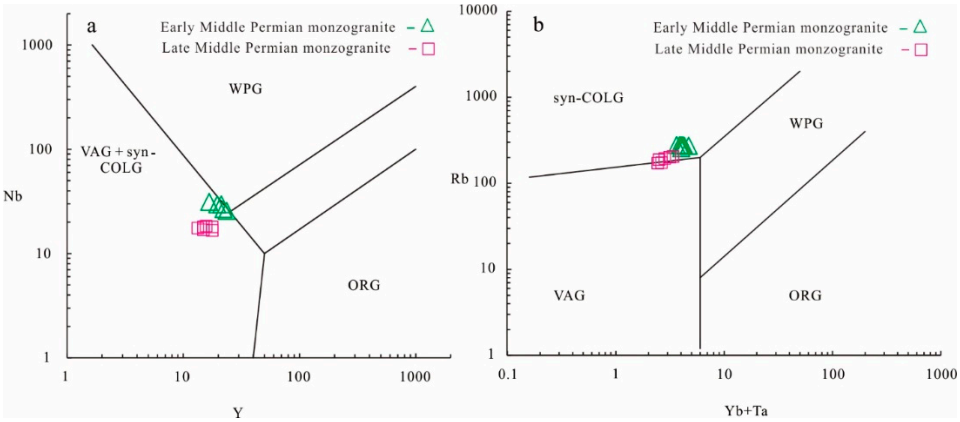

Figure 10. Identification diagram of tectonic setting for the Middle Permian granites in Chifeng area. (a) Y versus Nb, (b) Yb+Ta versus Rb; (after Pearce 1996), the fields are: ORG, oceanic ridge granites; syn-COLG, syn-collisional granites; VAG, volcanic arc granites; WPG, within-plate granites

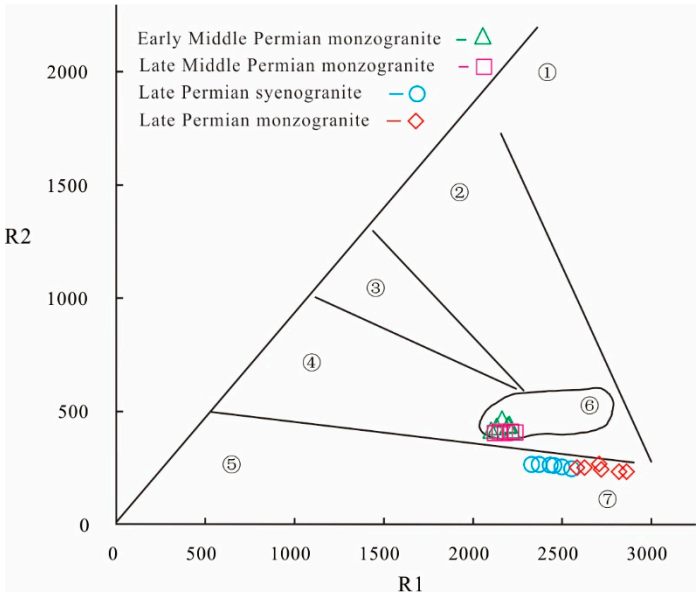

Figure 11. Diagram of R2 versus R1 for the Middle-Late Permian granites in Chifeng area. ① plagiogranite; ② active continental margin granite; ③ collisional-orogenic granite; ④ late orogenic granite; ⑤ unorogenic A-type granite; ⑥ collision granite (S-type); ⑦ post-orogenic granite;.

5.3.1.2. The tectonic setting of the Late Permian granite

Previous studies have shown that the Late Permian-Triassic magmatic rocks on the northern margin of the NCC show the characteristics of post-collision/post-orogeny magmatism in terms of rock assemblage, mineral composition, high-potassium and calc-alkaline-based geochemical characteristics, magmatic evolution, and isotope composition（Zhang et al.,2010；Shao et al.,2012; Chen et al., 2019, 2022b; Shi et al., 2022）. On the R1-R2 diagram(Figure 11), all the Late Permian granite fall within the range of post-orogenic granite, indicating that the granite in the study area may be related to the post-orogenic extension environment.

The Late Permian-Early Triassic granite in the Chifeng area consist of I-type granite and A-type granite, combined with available data, acidic members formed (256-248 Ma)（Shao et al.,2012；Duan et al.,2014；Liu et al.,2015; Chen et al., 2019）. The ophiolite formed from 256 to 246 Ma represents coeval basic members（Miao et al., 2008；Jian et al., 2010；Chu et al., 2013；Song et al., 2015）. “Bimodal volcanic rocks” appear between the northern margin of the NCC and the XMOB during the Late Permian-Early Triassic. Previous studies have shown that “bimodal volcanic rocks” can be formed under the following extensional environments: continental rift environment, oceanic island

Preprints (www.preprints.org) | NOT PEER-REVIEWED | Posted: 21 September 2023 doi:10.20944/preprints202309.1383.v1

extensional environment, destructive plate margin environment, post-orogenic extensional environment, oceanic island arc, mature island arc and initial back-arc basin environment（Ikeda and Yuasa, 1989； Pin and Paquette, 1997）. The Late Permian granitic rocks in the Chifeng area is dominated by middle-high potassium calc-alkaline type-I granite and A-type granite, indicating post-orogenic extensional environment（Hildreth et al., 1991； Eby et al.,1992； Turner et al., 1992； Frost et al., 1999； Bonin, 2004； Zhang et al., 2012）.

Late Permian granite is characterized by the enrichment of light rare earth elements and large ion lithophile elements and the depletion of high-field elements, and elements such as Nb, Ti, and P, showing the characteristics of the granite in the post-collision evolution stage of continental orogenic belts. Tectonic environment discriminant map(Figure 12a,b,c) shows that the granite from the Chifeng area all falls in the range of post-collision granite. In the Y+Nb-Rb and Yb+Ta-Rb diagram, all the samples fall in the post-collision range (Figure 12d,e).

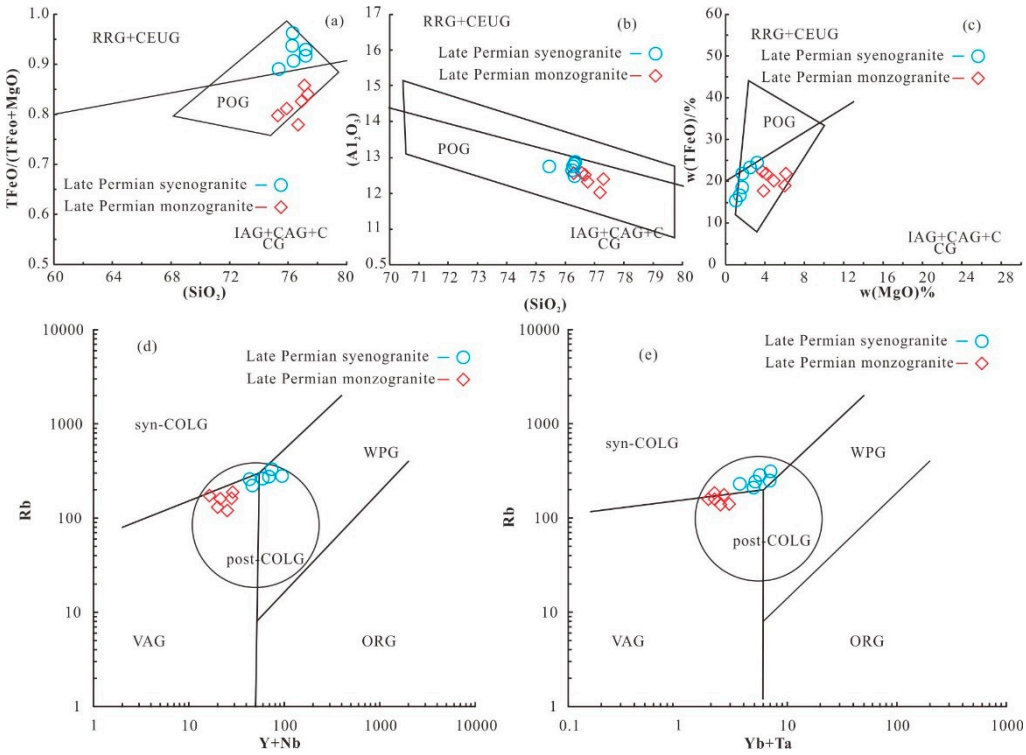

Figure 12. Identification diagram of tectonic setting for the Late Permian granites in Chifeng area. (a) TFeO/(TFeO+MgO) versus SiO_2(wt%); (b) Al_2O_2(wt%) versus SiO_2(wt%); (c) TFeO (wt%) versus MgO(wt%), IAG, island arc granite； CAG, continental arc granite； CCG, continental collision granite； POG, post- orogenic granite； RRG, rift related granite； CEUG, continental epeirogenetic uplift granite;(d) Yb+Nb versus Rb, (e) Yb+Ta versus Rb; (after Pearce 1996), the fields are: ORG, oceanic ridge granites; syn-COLG, syn-collisional granites; VAG, volcanic arc granites; WPG, within-plate granites.

The post-collisional is a complex period, usually starting after the closure of the main ocean, there are still large-scale horizontal block movement along the giant shear zone（Liegeois et al., 1998）. Most post-collision granites in orogenic belts are dominated by medium-high potassium calc-alkaline I-type granite, and there are also some S-type and A-type granite（Han.,2007）. The appearance of various types of rock assemblages shows the complexity and diversity of post-collision magmatism（Han.,2007； Zhang et al.,2010）. In a post collision environment, the pressure decreases under the action of extension, which is beneficial to rock melting. Mantle-derived magma underplated and asthenospheric mantle upwelled under the extensional thinning of the lithospheric crust. Sufficient heat source makes partial the crust melting further, and leading to the formation of a large number of acidic rocks. Therefore, the appearance of a large number of post-collision

 doi:10.20944/preprints202309.1383.v1

intermediate-acid igneous rocks may represent a transition from continental convergence to extension（Barbarin, 1999；Liegeois et al., 1998；）.

The following dynamic mechanisms may result in post-collision or post-orogenic magmatism: mantle convective thinning mode, gravity collapse, slab fragmentation mode, and delamination mode. As mentioned above, the Late Permian-Early Triassic intrusive rocks with post-orogenic characteristics constitute a long and narrow magmatic rock belt, which spreads along both sides of the deep fault zone in the middle section of the northern margin of the NCC. This distribution mode means that the Late Permian granite rocks in the study area are inferred to have been emplaced in an extensional environment caused by slab breaking-off after final closure of the PAO between the XMOB and the NCC（von Blanckenburg and Davies，1995；Chen et al., 2019）.

5.3.2. Permian Tectonic-Magmatic Evolution in the Chifeng Area

Chronological results show that there are three phases of tectonic-magmatism in the Permian in the Chifeng area. The rock assemblage, geochemical characteristics, genesis and tectonic setting of the granite from each phase were discussed in this paper. Combined with previous research, the Permian tectonic-magmatic evolution model were constructed(Figure 13). The specific dynamic process is as follows:

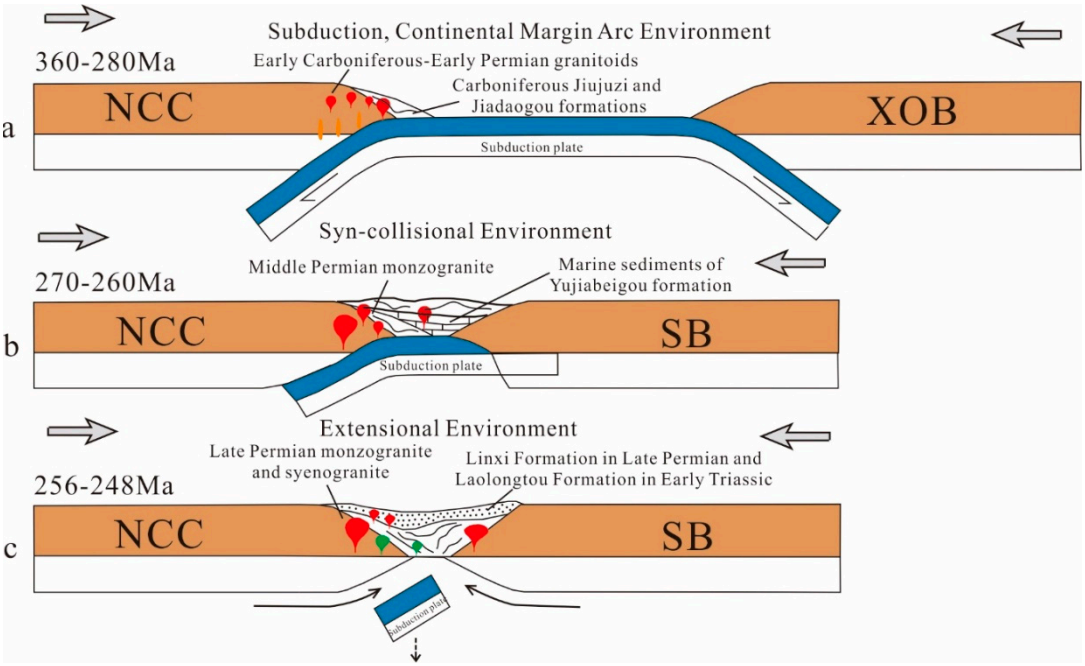

Figure 13. A tectonic evolution model from Carbonifreous to Permian in the north margin of the NCC in Chifeng-Aohan area. NCC, North China Craton; SB, Songliao Block.

5.3.2.1. Early Permian-active continental marginal environment

The Early Permian granite in the Chifeng area formed in an active continental margin environment under the background of the southward subduction of the PAO. The coeval volcanic rocks of the Permian Elitu Formation are also the products of the subduction environment（Li et al., 2018）.

Regionally, the PAO started to subduct southward from the late Early Carboniferous, and magmatic rocks from the Late Early Carboniferous to the Middle Permian showed active continental margins in terms of distribution, rock assemblages, mineral compositions, geochemical characteristics, and isotopes, also known as Andean active continental marginal arc（Xiao et al., 2003；Zhang et al., 2006，2007）. Results of the SHRIMP U-Pb ages and geochemistry of several granite intrusive rocks in the northern margin of NCC show that, the granite has the characteristics of calc-alkaline and subduction-related I-type granite, and the emplacement age is 300-320Ma, indicating

that there was an Andean continental arc in the northern margin of NCC , the PAO still existed in the Late Carboniferous-Early Permian, and it eventually closed later than 290Ma（Zhang et al., 2007）. Continous Late Carboniferous-Early Permian (324~274Ma) rock assemblages on the northern margin of the NCC were identified, such as horndiorite gabbro, diorite-quartz diorite, granodiorite, and granite. According to the geochemical characteristics of this group of intrusions, it is believed that the continental arc existing in the northern margin of the NCC lasted at least 50Ma（Zhang et al., 2009）. By studying the Early Permain granite in the Xilinhot, Li (2018) also confirmed the northern margin of the NCC was in continental marginal arc environment from the Late Carboniferous to the end of Early Peramin（Li et al., 2018）. By studying the granite in the Siziwang Banner, Wang Wanqiong (2014) considered the Early Permian quartz diorite formed in a continental marginal arc environment（Wang.,2014）. Li (2018) also argured that the Early Permian monzonitic and syenite granite in the western Chifeng area formed in continental marginal arc environment（Li et al.,2018）.

From the above researches, the middle section of the northern margin of the NCC was under the tectonic environment of the active continental margin, because of southward subduction of the PAO during the Early Carboniferous-Early Permian(Figure 13a). As a result, Andean-type active continental margin calc-alkaline rock assemblages of west-east trending formed along the northern margin of the NCC. Based on previous data, the existence of the Early Carboniferous-Early Permian intrusive rocks (358-280 Ma) with high potassium and calc-alkaline characteristics related to subduction implies that the subduction of the PAO lasted at least around 80Ma（Zhang et al., 2009a；Zhang et al., 2014；Li et al., 2018；Jiang et al.,2014；Wang.,2014）.

Therefore, the evidence of magmatic events indicated that there was a magmatic arc lasting about 80 Ma in the Jining-Chifeng area in the middle section of the northern margin of the NCC during the Early Carboniferous-Early Permian (358Ma～280Ma) (Figure 13a).The entire northern margin of the NCC should be in an active continental marginal environment under the subduction, indicating the PAO was not closed at that time.

5.3.2.2. Middle Permian-continent-continent collision environment

Geochemical characteristic show that the Middle Permian granite in the study area is monzogranite formed in a syn-collision environment, indicating that the XMOB collided with the NCC at this time(Figure 13b). The collisional granite were identified in Sonid Left Banner with an age of 230-250 Ma, which indicating that the PAO closed between 310 Ma and 230 Ma（Chen et al.,2000,2009）, implying the collision between the XMOB and the NCC lasted from the Middle Permain to the Middle-Late Triassic. Li Jinyi et al. (2007) discovered the granite with SHRIMP U-Pb ages of 229Ma and 237Ma. They considered it is S-type granite formed by the crystallization of younger crust remelted. The geochemical characteristics show that the Shuangjingzi intrusions were similar to syn-collisional granite, implying they were likely to emplace at the late collisional orogeny period. Therefore, it was concluded that the XMOB and the NCC began to collide along the Xra Moron suture zone at about 270 Ma and ended at 230 Ma（Li et al.,2007）.

During the early Middle Permian, the plant fossils in the Yujiabeigou Formation (the zircon age of crystalline tuff was 270 Ma) were all Cathaysian flora molecules, no mixing growth phenomenon, indicating the study area was Cathaysian flora distribution area. At that time, the Solonker-Xar Moron-Changchun-Yanji suture zone was not yet closed（Sun et al.,2016）, and the PAO developed into an intercontinental residual ocean basin. Subsequently, the oceanic crust disappeared, and continent-continent collision occurred, forming multiple Middle Permian syn-collision granitic intrusions. The gray-black slate and shale of the Linxi Formation from the Late Permian distributed in the southern margin of the Inner Mongolia are rich in freshwater bivalves, leaf limbs and plant fossils（Zhang et al.,2012）. With marine sediments at the bottom and delta-lacustrine-delta continental deposits in the middle-upper part, the Linxi Formation indicate two large plates had collided and collaged together, and jointly accepted the deposition during Late Permian.（Zhao et al.,2016）. The above evidences showed that the the northern margin of the NCC was in a co-collisional environment ,and the monzogranite formed in the Chifeng area.

During the Middle Permian, the Jining area in the middle section of the northern margin of the NCC was in a post-collisional environment（Zhang et al., 2007；Li et al., 2007；Wang.,2014；）, but the Yanbian area in the eastern section was in an active continental margin environment（Zhao et al.,2008；Yu et al.,2013）. The study area in this paper was between these two areas, so it was also in a co-collisional environment in the Middle Permian. This proved the PAO closed in a "scissor closure" mode from west to east.

5.3.2.3. Late Permian-Early Triassic-PAO final closure and subduction slab break-off

The granite of the Late Permian-Early Triassic was composed of A-type granite and I-type granite. They formed in a post-collisional extensional environment in response to the slab fragmentation after the collisional orogeny between the XMOB and the NCC(Figure 13c).

At present, there are still a lot of evidences to support that PAO was closed from the Late Permian to the Early Triassic. The buildup types, biota and tectonic activities on both sides of the Xra moron fault were obviously different during the Carboniferous-Permian. The paleobiogeographical flora appeared mixed up until the Middle or Late Permian（Huang and Ding.,1998）. Morever, the Linxi Formation from the Late Permian and the Xingfulu Formation from the Early Triassic were in a conformity contact, indicating that the study area was in the same tectonic environment from the Late Permian to the Early Triassic（Zhang et al.,2012）. There were continental deposits and terrestrial flora and fauna fossils in the Late Permian（Zhang et al.,2012）, indicating the two plate had collapsed and collaged and jointly accepted the deposition to form the Linxi Formation（Zhao et al.,2016）. Wang Yujing (2001) speculated that the final mixed accumulation time of the ophiolite belt was the Middle-Late Permian, according to age of the radiolarian in the siliceous rocks of the Xra Moron（Wang.,2001）. Both the biological extinction event and paleomagnetic evidence indicated that the PAO closed at the end of the Late Permian（Li et al., 2009）.

There were large quantities of intrusive rocks with continental margin arc magmatic character on the northern margin of the NCC, and with emplacement age ranged from 358Ma to 260Ma（Zhang et al., 2010；Zhang et al., 2007; Chen et al., 2018; Shi et al., 2019;）. The apperence of the post-collisional A-type granite and the "bimodal volcanic rocks" and the emplacement of the coeval ophiolite also indicated the PAO completely disappeared during the Permian-Early Triassic and finally closed along Xra Moron Suture Zone（Zhang et al.,2006；Miao et al., 2007；Song et al., 2015；Chen et al., 2019, 2022b; Shi et al., 2022）.

In summary, immediately after the Middle Permian continental collisional orogeny, the subducted slabs remaining in the lithospheric mantle experienced eclogite facies metamorphism and fragmented under the influence of gravity from the Late Permian to the Early Triassic (Figure 13c). The Chifeng area was in an extensional environment after the collision between the XMOB and the NCC. The crust occurred partial melting in response to the underplating of mantle-derived magma, the upwelling of deep asthenospheric mantle materials, increasing heat and decreasing pressure. As a result, the post-collisional A-type granite of west-east trending, "bimodal volcanic rock" and ophiolite formed during Late Permian-Early Triassic. The lacustrine Linxi Formation had abundant freshwater bivalves and the gray-black slate and shale containing leaf limbs and plant fossils（Zhao et al.,2016）. In addition, the paleobiogeographical divisions disappeared. All of these indicated the PAO finally closed along the Solonker-Xar Moron-Changchun-Yanji Suture (SXCYS) during Late Permian-Early Triassic and ocean basin disappeared completely(Chen et al., 2019, 2022b; Shi et al., 2022).

6. Conclusions

Based on the geological and petrological studies of the Permian granitic rocks in the Chifeng area, by analyzing the zircon U-Pb chronology, major and trace elements, combined with the related research on the northern margin of the NCC, the following conclusions were obtained:

(1) According to the zircon U-Pb dating, three stages of Permian granitic magmatism were identified in the Chifeng area: 1) an intrusive suite of syenogranite and monzogranite at 294-284 Ma,

2) a suite of monzogranites at 269-260 Ma, and 3) an intrusive suite of monzogranites and syenogranite at 256-254 Ma.

(2) The two phases of the Middle Permian monzogranite belong to the I-type granite with Al saturated, Si, K rich, negative anomaly of Eu, enrichment of LILEs (Rb, Th, K, La), negative Sr, P, Ti anomalies. The Late Permian syenite granite is rich in Si, K and poor in Al, belong to the I-type granite with moderate negative Eu anomalies, enrichment of LILEs (Rb, Th, K, La, Ce) and slightly enrichment in HFSEs (Nd, Zr, Hf), negative anomalies of Ba, P, Ti, and Sr. These Permian high-K I-type granites were formed by partial melting of lower crustal source under a relatively low-pressure condition. The Late Permian monzogranite belongs to the A-type granite, displaying a "swallow like" four group effect of rare earth elements, with strong negative Eu anomalies, enrichment of LILES (Rb, Th, U, K), negative anomalies of Ba, P, Ti, and obvious Sr negative anomalies, forming in a low-pressure environment caused by tension.

(3) The Pernian tectonic evolution of the PAO can be divided into three stages: 1)Early Permian granite formed in the setting of PAO subducting to the NCC, and the subduction lasted about 80 Ma; 2)Middle Permian granite formed in syn-collisional setting of the XMOB and the NCC; and3)Late Permian- Early Triassic granite formed in the extensional setting of the subducting slab breaking off after the collision between the XMOB and the NCC, the PAO finally closed.

Supplementary Materials: The following supporting information can be downloaded at the website of this paper posted on Preprints.org. Table S1. LA-ICP-MS zircon U-Pb data for the Permian granites in the Chifeng area; Table S2. Major (wt%) and trace (ppm) elements data of Permian granites in the Chifeng area.

Acknowledgments: We appreciate the editor and two anonymous reviewers for their constructive comments. Thanks to MDPI Editing Services for English language editing of this manuscript. We thank the staff of the Geologic Lab Center, China University of Geosciences (Beijing) and the Zhongnan Mineral Supervision and Testing Center of the Ministry of Land and Resources, for their advice and assistance during zircon U-Pb dating by LA-ICP-MS. We also appreciate the Northeast China Supervision and Inspection Center of Mineral Resources, Ministry of Land and Resources, Shenyang, China, for their assistance in the major and trace element analysis. This work was financially supported by the China Geological Survey (Grants DD20230004, DD20190042 and DD20160048-05).

References

1. Andersen, T. (2002). Correction of common Lead in U-Pb analyses that do not report ^{204}Pb. *Chemical Geology*, 192, 59–79.
2. Anderson, J.L. (1983). Proterozoic anorogenic granite plutonism of North America. *Memoir of the Geological Society of America*, 161, 133-154.
3. Belousova, E., Griffin, W., O'Reilly, S. Y., & Fisher, N. (2002). Igneous zircon: trace element composition as an indicator of source rock type. *Contributions to Mineralogy & Petrology*, 143(5), 602-622.
4. Bonin, B. (2004). Do coeval mafic and felsic magmas in post-collisional to within-plate regimes necessarily imply two contrasting, mantle and crustal, sources? A review. *Lithos*, 78(1): 1-24.
5. Cao, H.H., Xu, W.L., Pei, F.P., & Zhang, X. Z. (2011). Permian tectonic evolution in southwestern Khanka massif: Evidence from zircon U-Pb chronology, Hf isotope and geochemistry of gabbro and diorite. *Acta Geologica Sinica (English Edition)*, 85(6), 1390-1402.
6. Chappell, B.W., & White, A.J. (1992). I- and S-type granites in the Lachlan Fold Belt. *Transactions of the Royal Society of Edinburgh: Earth Sciences*, 83(1-2), 1-26.
7. Chen, B., Jahn, B.M., & Tian, W. (2009). Evolution of the Solonker Suture Zone: Constraints from zircon U-Pb ages, Hf isotopic ratios and whole-rock Nd-Sr isotope compositions of subduction- and collision-related magmas and forearc sediments. *Journal of Asian Earth Sciences*, 34(3), 245–257.
8. Chen, B., Jahn, B.M., Wilde, S.A., & Xu, B. (2000). Two contrasting Paleozoic magmatic belts in northern Inner Mongolia, China: Petrogenesis and tectonic implications. *Tectonophysics*, 328(1), 157–182.
9. Chen, J. S., Li, B., Yang, H., Liu, M., Yang, F., Li, W., Wang, Y., & Cui, T. R. (2018). New Zircon U-Pb Age of Granodiorite in Chifeng at the Northern Margin of North China Craton and Constraints on Plate Tectonic Evolution. *Acta Geologica Sinica (English Edition)*, 92(1), 410–413.
10. Chen, J. S., Li, W. W., Shi, Y., Li, B., Zhao, C.Q., & Zhang, L. D. (2022b). Evolution of the eastern segment of the the northern margin of the North China Craton in the Triassic: Evidence from the geochronology and

geochemistry of magmatic rocks in Kaiyuan area, North Liaonign. *Acta Petrologica Sinica*, 38(8), 2216-2248 (in Chinese with English abstract).

11. Chen, J.S., Liu, Z. H., Liu, Y. J., Feng, Z. Q., Zhang, L. D., & Wang, Y. (2022a). Evolution of the eastern segment of the the northern margin of the North China Craton in the Triassic: Evidence from the geochronology and geochemistry of magmatic rocks in Kaiyuan area, North Liaonign. *Acta Petrologica Sinica*, 38(8) ,2175-2180 (in Chinese with English abstract).
12. Chen, J.S., Tian, D.X., Yang, H., Li, W.W., Liu, M., Li, B., Yang, F., Li, W & Wu, Z. (2019). Triassic granitic magmatism at the northern margin of the North China Craton: Implications of geochronology and geochemistry for the tectonic evolution of the Central Asian Orogenic Belt. *Acta Geologica Sinica (English Edition)*, 93(5), 1325–1353. DOI:10.1111/1755-6724.14350
13. Chu, H., Zhang, J.R., Wei, C.J., Wang, H. C., & Ren, Y. W. (2013). A new interpretation of the tectonic setting and age of meta-basic volcanics in the Ondor Sum Group, Inner Mongolia, China. *Science Bulletin*, 58, 3580–3587.
14. Clemens, J. D., Darbyshire, D. P. F., & Flinders, J. (2009). Sources of post-orogenic calcalkaline magmas: the Arrochar and Garabal Hill-Glen Fyne complexes, Scotland. *Lithos*, 112, 524-542.
15. Clemens, J.D., Holloway, J.R., & White, A.J. (1986). Origin of A-type granites: Experimental constraints. *American Mineral*, 71, 317 -324 .
16. DePaolo, D. J. (1981). Trace element and isotopic effects of combined wallrock assimilation and fractional crystallization. *Earth & Planetary Science Letters*, 53, 189-202.
17. Dickinson, W. R. (1975). Potash-depth (K-h) relations in continental-margin and intraoceanic magmatic arcs. *Geology*, 3, 53-56.
18. Duan, P.X., Li, C.M., Liu, C., Deng, J. F., & Zhao, G. C. (2014). Geochronology and geochemistry of the granites from the Jinchanggouliang gold deposit area in the Inner Mongolia and its geological significance. *Acta Petrologica Sinica*, 30(11), 3189–3202 (in Chinese with English abstract).
19. Eby, G.N. (1992). Chemical subdivision of the A-type granitoids: Petrogenetic and tectonic implications. *Geology*, 20, 641–644.
20. Frost, C.D., Frost, B.R., Chamberlain, K.R., & Edwards, B. R. (1999). Petrogenesis of the 1.43 Ga Sherman batholith, SE Wyoming, USA: A reduced, rapakivi-type anorogenic granite. *Journal of Petrology*, 40(12), 1771-1802.
21. Guan, Q. B., Liu, Z. H., Liu, Y. J., Liu, J., Wang, S. J., & Tian, Y. 2019. Geochemistry and zircon U–Pb geochronology of mafic rocks in the Kaiyuan tectonic mélange of northern Liaoning Province, NE China: Constraints on the tectonic evolution of the Paleo-Asian Ocean. *Geological Journal*, 54(2): 656-678, doi: 10.1002/gj.3442
22. Han, B.F. (2007). Diverse post-collisional granitoids and their tectonic setting discrimination. *Earth Science Frontiers*, 14(3), 64-72.(in Chinese with English abstract).
23. Hildreth, W.E., Halliday, A.N., & Christiansen, R.L. (1991). Isotopic and chemical evidence concerning the genesis and contamination of basaltic and rhyolitic magma beneath the Yellowstone Plateau Volcanic Field. *Journal of Petrology*, 32(1), 63-138.
24. Hofmann, A. W. (1988). Chemical differentiation of the Earth: the relationship between mantle, continental crust, and oceanic crust. *Earth & Planetary Science Letters*, 90, 297-314.
25. Hoskin, P.W.O., & Ireland, T.R. (2000). Rare earth element chemistry of zircon and its use as a provenance indicator. *Geology*, 28(7), 627–630.
26. Huang, B.H., & Ding, Q.H. (1998). The angara flora from Northern China. *Acta Geoscientia Sinica*, 19(1), 97–104 (in Chinese with English abstract).
27. Ikeda, Y., & Yuasa, M. (1989). Volcanism in Nascent backarc basins behind the Schichito ridge and adjacent areas in the Izu-Ogasawara Arc, NW Pacific; Evidence for mixing between E-type MORB and island arc magmas at the initiation of back-arc rifing. *Contributions to Mineralogy and Petrology*, 101, 377-393.
28. Jahn, B.M. (2004). The Central Asian Orogenic Belt and growth of the continental crust in the Phanerozoic. *Geological Society, London, Special Publications*, 226, 73–100.
29. Jian, P., Liu, D.Y., KröNer, A., Windley, B. F., Shi, Y. R., Zhang, W., Zhang, F. Q., Miao, L. C., Zhang, L. Q., & Tomurhuu, D. (2010). Evolution of a Permian intraoceanic arc-trench system in the Solonker Suture Zone, Central Asian Orogenic Belt, China and Mongolia. *Lithos*, 118(1–2), 169–190.

30. Jiang, S.H., Liang, Q.L., Nie, F.J., & Liu, Y. F. (2014). A preliminary study of zircon LAMC-ICP-MS U-Pb ages of the Shuangjingzi complex in Linxi, Inner Mongolia. *Geology in China*, 41(4), 1108–1123 (in Chinese with English abstract).
31. Li, B., Chen, J.S., Liu, M., Yang, F., Li, W., Wu, Z., Chen, M. H., & Wu, C. S. (2018). LA-ICP-MS zircon U-Pb geochronology and geochemical characteristics of the Early Permian granite in Chifeng area, Inner Mongolia. *Geological Bulletin of China*,37(9), 1671-1681(in Chinese with English abstract).
32. Li, J.Y. (2006). Permian geodynamic setting of northeast China and adjacent regions: Closure of the Paleo-Asian Ocean and subduction of the Paleo-Pacific Plate. *Journal of Asian Earth Sciences*, 26(3–4), 207–224.
33. Li, J.Y., Gao, L.M., Sun, G.H., Li, Y. P., & Wang, Y. B. (2007). Shuangjingzi Middle Triassic syn-collisional crust-derived granite in the East Inner Mongolia and its constraint on the timing of collision between Siberian and Sino-Korean Paleo-plates. *Acta Petrologica Sinica*, 23(3), 565–582 (in Chinese with English abstract).
34. Li, P.W., Gao, R., Guan, Y., & Li, Q. S. (2009). The closed times of the Paleo-Asian Ocean and the Paleo-Tethys Ocean: Implication for the tectonic cause of the End-Permian mass extinction. *Journal of Jilin University(Earth Science Edition)*, 39(3), 521–527 (in Chinese with English abstract).
35. Li, X.H., Qi, C.S., & Liu, Y. (2005). Petrogenesis of the Neoproterozoic bimodal volcanic rocks along the western margin of Yangtze Block: New constranits from Hf isotopes and Fe/Mn ratios. *Chinese Science Bulletin*, 50: 2481–2486.
36. Liegeois, J.P., Navez, J., Hertogen, J., & Black, R. (1998). Contrasting origin of postcollisional high-K calc-alkaline and shoshonitic versus alkaline and peralkaline granitoids: the use of sliding normalization. *Lithos*, 45, 1–28.
37. Liu, Y., Xi, A.H., Ge, Y.H., Tang, X. Y., Xu, B. W., Wang, M. Z., & Ma, Y. J. (2015). LA-ICP-MS zircon U-Pb ages and petrogenesis of granodiorite in Mengguyingzi, Chifeng, Inner Mongolia. *Geological Bulletin of China*, 34(2/3), 437–446 (in Chinese with English abstract).
38. Liu, Y.J., Li, W.M., Feng, Z.Q., Wen, Q. B., Neubauer, F., & Liang, C.Y. (2017). A review of the Paleozoic tectonics in the eastern part of Central Asian Orogenic Belt. *Gondwana Research*, 43, 123–148.
39. Ludwig, K.R. (2003). User's manual for isoplot 3.0: A geochronological toolkit for microsoft excel. *Berkeley Geochronology Center Special Publication*, 4, 1–70.
40. Miao, L.C., Fan, W.M., Liu, D.Y., Zhang, F. Q., Shi, Y. R., & Guo, F. (2008). Geochronology and geochemistry of the Hegenshan ophiolitic complex: Implications for late-stage tectonic evolution of the Inner Mongolia-Daxinganling Orogenic Belt, China. *Journal of Asian Earth Sciences*, 32(5), 348–370.
41. Miao, L.C., Zhang, F.Q., Fan, W.M., & Liu, D. Y. (2007). Phanerozoic evolution of the Inner Mongolia-Daxinganling Orogenic Belt in North China: Constraints from geochronology of ophiolites and associated formations. *Geological Society London Special Publications*, 280(1), 223–237.
42. Moghazi, A. M. (2003). Geochemistry and petrogenesis of a high-K calc-alkaline Dokhan Volcanic suite, South Safaga area, Egypt: the role of late Neoproterozoic crustal extension. *Precambrian Research*,125, 161-178.
43. Pin, C., & Paquette, J.L. (1997). A mantle-derived bimodal suite in the Hercynian belt: Nd isotope and trace element evidence for a subduction-related rift origin of the Late Devonian brevenne metavolcanics, Massif Central (France). *Contributions to Mineralogy and Petrology*, 129, 222-238.
44. Rickwood, P. C. (1989). Boundary lines within petrologic diagrams which use oxides of major and minor elements. *Lithos*, 22(4), 247-263.
45. Roberts, M. P., & Clemens, J. D. (1993). Origin of high-potassium, calc-alkaline, I-type granitoids. *Geology*, 21, 825-828.
46. Robinson, P.T., Zhou, M.F., Hu, X.F., Reynolds, P., Bai, W. J., & Yang, J. S. (1999). Geochemical constraints on the oringin of the Hegenshan opheiolite, Inner Mongolia, China. *Journal of Asian Earth Sciences*, 17, 423–442.
47. Scaillet, B., & Macdonald, R. (2001). Phase relations of peralkaline silicic magmas and petrogenetic implications. *Journal of Petrology*, 42, 825 -845 .
48. Scaillet, B., & Macdonald, R. (2003). Experimental constraints on the relationships between peralkaline rhyolites of the Kenya Rift Valley. *Journal of Petrology*, 44(10), 1 867-1 894 .
49. Sengör, A.M.C., & Natal'in, B.A. (1996). Paleotectonics of Asia: Fragments of a synthesis[M]//Yin A, Harrison T M. The tectonic evolution of Asia. *Cambridge: Cambrige University Press*, 486–641.

50. Sengör, A.M.C., Natal'in, B.A., & Burtman, V.S. (1993). Evolution of the altaid tectonic collage and Palaeozoic crustal growth in Eurasia. *Nature*, 364, 299–307.
51. Shao, J.A., Zhang, Z., She, H.Q., & Liu, D. S. (2012). The discovery of Phanerozoic granulite in Chifeng area of North Craton and its implication. *Earth Science Frontiers*, 19(3), 187–198 (in Chinese with English abstract).
52. Shi, S.S., Shi, Y., Zhang, C., Shi, J. M., & Jiang, S. 2022. Geochronology and geochemistry of the Triassic intrusive rocks in the Faku area, northern Liaoning, China: Constraints on the evolution of the Palaeo-Asian Ocean. *Geological Journal*, 57(4): 1658-1681, doi: 10.1002/gj.4368
53. Shi, Y., Shi, S. S., Liu, Z. H., Liu, J., Ju, N., You, H. X., Zhang, Z. B., & Zhao, C. Q. 2019. Petrogenesis of the late Early Palaeozoic adakitic granitoids in the southern margin of the Songliao Basin, NE China: Implications for the subduction of the Palaeo-Asian Ocean. *Geological Journal*, 54(6): 3821-3839
54. Sisson, T. W., Ratajeski, K., Hankins, W. B., & Glazner, A. F. (2005). Voluminous granitic magmas from common basaltic sources. *Contributions to Mineralogy & Petrology*, 148, 635-661.
55. Song, S.G., Wang, M.M., Xu, X., Wang, C., Niu, Y. L., Allen, M. B., & Su, L. (2015). Ophiolites in the Xing'an-Inner Mongolia accretionary belt of the CAOB: Implications for two cycles of seafloor spreading and accretionary orogenic events. *Tectonics*, 34(10), 2221–2248, doi: 10.1002/2015TC003948.
56. Springer, W., & Seck, H. A. (1997). Partial fusion of basic granulites at 5-15 kbar: implications for the origin of TTG magmas. *Contributions to Mineralogy & Petrology*, 127 (1-2): 30-45.
57. Sun, S.S., & McDonough, W.F. (1989). Chemical and isotopic systematics of oceanic basalts: Implications for mantle composition and processes. *Geological Society, London, Special Publications*, 42 (1), 313–345.
58. Sun, Y.W., Ding, H.S., Liu, H., Zhang, D. J., Gong, F. H., & Zheng, Y. J. (2016). Fossil plants from the Guadalupian Yujiabeigou Formation in the north margin of North China Plate and their tectonic implications. *Journal of Jilin University(Earth Science Edition)*, 46(5), 1268-1283. (in Chinese with English abstract).
59. Tang, K.D. (1990). Tectonic development of Paleozoic fold belts at the northern margin of the Sino-Korean Craton. *Tectonics*, 9, 249–260.
60. Tang, K.D., Ju, N., Zhang, D.Q., Zhang, G.B., Feng, Y., & Sun, J.G. (2022). Implication of the tectonic eveolution of Paleo-Asian Ocean. *Geology and Resources*, 31(3), 246-259 (in Chinese with English abstract)
61. Tian, S.G., Li, Z.S., Zhang, Y.S., Gong, Y. X., Zhai, D. X., & Wang, M. (2016). Late Carboniferous-Permian tectono-geographical conditions and development in eastern Inner Mengolia and adjacent areas. *Acta Geologica Sinica* , 90(4), 688-707.(in Chinese with English abstract).
62. Topuz, G., Altherr, R., Siebel, W., Schwarz, W. H., Zack, T., Hasözbek, A., Barth, M., Satır, M., & Şen, C. (2010). Carboniferous high-potassium I-type granitoid magmatism in the Eastern Pontides: the Gümüşhane pluton (NE Turkey). *Lithos*, 116, 92-110.
63. Turner, S., Sandiford, M., & Foden. J. (1992). Some geodynamic and compositional constraints on "postorogenic" magmatism. *Geology*, 20(10), 931-934.
64. Von Blanckenburg, F., & Davies, J.H. (1995). Slab breakoff: A model for syncollisional magmatism and tectonics in the Alps. *Tectonics*, 14(1), 120-131.
65. Wang, Q., & Liu, X.Y. (1986). Paleoplate tectonics between Cathasia and Angaraland in Inner Mongolia of China. *Tectonics*, 5(7), 1073-1088.
66. Wang, Y.J. (2001). A review of the study of the Palaeozoic radiation of the Palaeozoic in China. *Acta Micropalaeontological Sinica*, 18(4), 313–320 (in Chinese with English abstract).
67. Wang, W.Q. (2014). Late Paleozoic tectonic evolution of the central-northern margin of the North China Craton: Constraints from zircon U-Pb ages and geochemistry of igneous rocks in Ondor Sum-Jining area. *Jilin University*, 1–169 (in Chinese with English abstract).
68. Wiedenbeck, M., Allé, P., Corfu, F., Griffin, W. L., & Spiegel, W. (2007). Three natural zircon standards for U-Th-Pb, Lu-Hf, trace element and REE analyses. *Geostandards and Geoanalytical Research*, 19(1), 1–23.
69. Windley, B.F., Alexeiev, D., Xiao, W.J., Kroener, A., & Badarch, G. (2007). Tectonic models for accretion of the Central Asian Orogenic Belt. *Journal of the Geological Society London*, 164, 31–48.
70. Wu, F.Y., Sun, D.Y., Ge, W.C., Zhang, Y. B., Grant, M. L., Wilde, S. A.,& Jahn, B. M. (2011). Geochronology of the Phanerozoic granitoids in northeastern China. *Journal of Asian Earth Sciences*, 41, 1–30.
71. Wu, F.Y., Sun, D.Y., Li, H.M., Jahn, B. M., & Wilde, S. A. (2002). A-type granites in northeastern China: Age and geochemical constraints on their petrogenesis. *Chemical Geology*, 187(1), 143–173.

72. Xi, A.H., Ma, Y.J., Ge, Y.H., Tang, X. Y., Liu, S., Xu, B. W., & Liu, Y. (2015). Multi-stage intrusive evidence and geological significance of Dayingzi granite in Chifeng, eastern Inner Mongolia. *Journal of Jilin University (Earth Science Edition)*, 45(3), 791-803.(in Chinese with English abstract).
73. Xiao, W.J., Windley, B.F., Hao, J., & Zhai, M. G. (2003). Accretion leading to collision and the Permian Solonker Suture, Inner Mongolia, China: Termination of the Central Asian Orogenic Belt. *Tectonics*, 22(6), 1069–1090.
74. Yang, H., Ge, W. C., Zhao, G. C., Dong, Y., Xu, W. L., Wang, Z. H., Ji, Z., & Yu, J. J. (2015). Late Triassic intrusive complex in the Jidong region, Jiamusi-Khanka Block, NE China: geochemistry, zircon U-Pb ages, Lu-Hf isotopes, and implications for magma mingling and mixing. *Lithos*, 224-225, 143-159.
75. Yang, J. H., Wu, F. Y., Chung, S. L., Wilde, S. A., & Chu, M. F. (2006). A hybrid origin for the Yianshan A-type granite, northeast China: geochemical and Sr-Nd-Hf isotopic evidence. *Lithos*, 89, 89-106.
76. Yu, J. J., Wang, F., Xu, W. L., Gao, F. H., & Tang, J. 2013. Late Permian tectonic evolution at the southeastern margin of the Songnen-Zhangguangcai Range Massif, NE China: Constraints from geochronology and geochemistry of granitoids. *Gondwana Research*, 24(2), 635-647
77. Zhang, Q., Ran, A., & Li, C.D. (2012). A-type granite: What is the essence?. *Acta Petrologica Et Mineralogica*, 31(4), 621–626 (in Chinese with English abstract).
78. Zhang, S.H., Zhao, Y., & Song, B. (2006). Hornblende thermobarometry of the Carboniferous granitoids from the Inner Mongolia Paleo-Uplift: Implications for the geotectonic evolution of the northern margin of North China Block. *Mineralogy and Petrology*, 87, 123-141 .
79. Zhang, S.H., Zhao, Y., Davis, G.A., Ye, H., & Wu, F. (2014). Temporal and spatial variations of Mesozoic magmatism and deformation in the North China Craton: Implications for lithospheric thinning and decratonization. *Earth-Science Reviews*, 131, 49–87.
80. Zhang, S.H., Zhao, Y., Kroner, A., Liu, X. M., Xie, L. W., & Chen, F. K. (2009). Early Permian plutons from the northern North China Block: Constraints on continental arc evolution and convergent margin magmatism related to the Central Asian Orogenic Belt. *International Journal of Earth Sciences*, 98(6), 1441-1467.
81. Zhang, S.H., Zhao, Y., Liu, J.M., Hu, J. M., Song, B., Liu, J., & Wu, H. (2010). Geochronology, geochemistry and tectonic setting of the Late Paleozoic-Early Mesozoic magmatism in the northern margin of the North China Block: A preliminary review. *Acta Petrologica Et Mineralogica*, 29(6), 824–842 (in Chinese with English abstract).
82. Zhang, S.H., Zhao, Y., Song, B., Hu, J. M., Liu, S. W., Yang, Y. H., Chen, F. K., Liu, X. M., & Liu, J. (2009a). Contrasting Late Carboniferous and Late Permian-Middle Triassic intrusive suites from the northern margin of the North China Craton: Geochronology, petrogenesis, and tectonic implications. *Geological Society of America Bulletin*, 121, 181–200.
83. Zhang, S.H., Zhao, Y., Song, B., Yang, Z. Y., Hu, J. M., & Wu, H. (2007). Carboniferous granitic plutons from the northern margin of the North China Block: Implications for a Late Palaeozoic active continental margin. *Journal of the Geological Society, London*, 164, 451–463.
84. Zhang, S.H., Zhao, Y., Ye, H., Hou, K. J., & Li, C. F. (2012). Early Mesozoic alkaline complexes in the northern North China Craton: Implications for cratonic lithospheric destruction. *Lithos*, 155, 1–18.
85. Zhang, Y.B., Wu, F.Y., Wilde, S.A., Zhai, M. G., Lu, X. P., & Sun, D. Y. (2004). Zircon U-Pb ages and tectonic implications of "Early Paleozoic" granitoids at Yanbian, Jilin Province, Northeast China. *The Island Arc*, 13, 484–505.
86. Zhao, P., Jahn, B., Xu, B., Liao, W., & Wang, Y. (2016). Geochemistry, geochronology and zircon Hf isotopic study of peralkaline-alkaline intrusions along the northern margin of the North China Craton and its tectonic implication for the southeastern Central Asian Orogenic Belt. *Lithos*, 92-108, doi:10.1016/j. *Lithos*.2015.12.013.
87. Zhao, Y. L., Li, W. M., Wen, Q.B., Liang, T. Y., Feng, Z. Q., Zhou, J. P., & Shen, L. (2016). Late Paleozoic tectonic framework of eastern Inner Mongolia: Evidence from the detrital zircon U-Pb ages of the Mid-Late Permian to Early Triassic sandstones. *Acta Petrologica Sinica*, 32(9), 2807–2822 (in Chinese with English abstract).